

Supporting information to  
**Flexibility is the Key to Tuning the Transport  
Properties of Fluorinated Imide-Based Ionic  
Liquids**

Frederik Philippi<sup>a</sup>      Daniel Rauber<sup>b</sup>      Oriele Palumbo<sup>c</sup>  
Kateryna Goloviznina<sup>d,e</sup>      Jesse McDaniel<sup>f</sup>      David Pugh<sup>g</sup>  
Sophia Suarez<sup>h</sup>      Carla C. Fraenza<sup>i</sup>      Agilio Padua<sup>d</sup>  
Christopher W. M. Kay<sup>b,j</sup>      Tom Welton<sup>a</sup>

May 31, 2022

<sup>a</sup> Department of Chemistry, Molecular Sciences Research Hub, Imperial College London, White City Campus, London W12 0BZ, United Kingdom.

<sup>b</sup> Department of Chemistry, Saarland University, Campus B2.2, Saarbrücken, Germany.

<sup>c</sup> Consiglio Nazionale delle Ricerche, Istituto dei Sistemi Complessi, Piazzale Aldo Moro 5, 00185 Rome, Italy.

<sup>d</sup> Laboratoire de Chimie, École Normale Supérieure de Lyon & CNRS, 69364 Lyon, France.

<sup>e</sup> current address: Sorbonne Université, CNRS, Physico-chimie des Électrolytes et Nanosystèmes Interfaciaux, PHENIX, F-75005 Paris, France.

<sup>f</sup> School of Chemistry and Biochemistry, Georgia Institute of Technology, Atlanta, Georgia, 30332-0400, USA

<sup>g</sup> Department of Chemistry, King's College London, 7 Trinity Street, London SE1 1DB, UK.

<sup>h</sup> Department of Physics, Brooklyn College of CUNY, Brooklyn, New York, 11210, USA.

<sup>i</sup> Department of Physics and Astronomy, Hunter college of CUNY, New York, 10065, USA.

<sup>j</sup> London Centre for Nanotechnology, University College London, 17-19 Gordon Street, London WC1H 0AH, United Kingdom.

# Contents

<b>1</b>	<b>Ab initio</b>	<b>4</b>
<b>2</b>	<b>Syntheses</b>	<b>7</b>
2.1	Precursors . . . . .	9
2.1.1	H[NMs <sub>2</sub> ] . . . . .	9
2.1.2	H[TfNAc] . . . . .	9
2.1.3	H[NMsTFA] . . . . .	10
2.1.4	H[NTfMs] . . . . .	10
2.1.5	Na[NMsTFA] . . . . .	10
2.1.6	Na[TfNAc] . . . . .	11
2.1.7	TfNHK . . . . .	11
2.1.8	Li[NTfMs] . . . . .	11
2.1.9	[C <sub>4</sub> C <sub>1</sub> im]Cl . . . . .	12
2.1.10	[N1111][NMs <sub>2</sub> ] . . . . .	12
2.2	Ionic Liquids . . . . .	13
2.2.1	[C <sub>4</sub> C <sub>1</sub> im][6cPFSI] . . . . .	13
2.2.2	[C <sub>4</sub> C <sub>1</sub> im][NTf <sub>2</sub> ] . . . . .	13
2.2.3	[C <sub>4</sub> C <sub>1</sub> im][NMs <sub>2</sub> ] . . . . .	14
2.2.4	[C <sub>4</sub> C <sub>1</sub> im][B(CN) <sub>4</sub> ] . . . . .	14
2.2.5	[C <sub>4</sub> C <sub>1</sub> im][CHTf <sub>2</sub> ] . . . . .	15
2.2.6	[C <sub>4</sub> C <sub>1</sub> im][NTfAc] . . . . .	15
2.2.7	[C <sub>4</sub> C <sub>1</sub> im][NTfMs] . . . . .	16
2.2.8	[C <sub>4</sub> C <sub>1</sub> im][NMsTFA] . . . . .	16
<b>3</b>	<b>Single Crystal XRD</b>	<b>17</b>
<b>4</b>	<b>Physical Chemistry</b>	<b>22</b>
4.1	Comparison with Literature Data . . . . .	22
4.2	Thermal Transitions . . . . .	22

4.3	Density . . . . .	23
4.4	Viscosity . . . . .	25
4.5	Conductivity . . . . .	27
4.6	Diffusion Coefficients . . . . .	31
4.7	DMTA Measurements . . . . .	32
<b>5</b>	<b>MD simulations</b>	<b>37</b>
5.1	MD simulation details . . . . .	37
5.2	Force Field . . . . .	38
5.3	Structure, Diffusion, and Heterogeneity . . . . .	43
5.4	Time Correlation Functions . . . . .	47
5.5	Conformational Space . . . . .	49
5.6	Charge Arm ("Dipole Moment") . . . . .	50
5.7	Charge Network relaxation times . . . . .	52

# 1 Ab initio

Previously unpublished (stationary point and PES) data are given in Table 1 and in Figure 1, Figure 2 and Figure 3.

Table 1: Geometries and energies for additional stationary points. GS = Ground State = minimum energy geometry, TS = Transition State = first order saddle point.

System		$\phi^1$ / degrees	$\phi^2$ / degrees	Energy / kJ mol <sup>-1</sup>
[C(CN)Tf <sub>2</sub> ] <sup>-</sup>	GS	88	88	0.0
[C(CN)Tf <sub>2</sub> ] <sup>-</sup>	GS	83	252	8.5
[C(CN)Tf <sub>2</sub> ] <sup>-</sup>	TS	98	262	9.7
[C(CN)Tf <sub>2</sub> ] <sup>-</sup>	TS	94	178	39.0
[C(CN)Tf <sub>2</sub> ] <sup>-</sup>	TS	358	94	51.5
[N(SO <sub>2</sub> CN) <sub>2</sub> ] <sup>-</sup>	GS	75	75	0.0
[N(SO <sub>2</sub> CN) <sub>2</sub> ] <sup>-</sup>	GS	63	248	8.4
[N(SO <sub>2</sub> CN) <sub>2</sub> ] <sup>-</sup>	TS	83	277	11.4
[N(SO <sub>2</sub> CN) <sub>2</sub> ] <sup>-</sup>	TS	80	150	19.1
[N(SO <sub>2</sub> CN) <sub>2</sub> ] <sup>-</sup>	TS	2	79	23.9
[NTfMs] <sup>-</sup>	GS	88	65	0.0
[NTfMs] <sup>-</sup>	GS	242	58	1.5
[NTfMs] <sup>-</sup>	TS	88	0	10.7
[NTfMs] <sup>-</sup>	GS	280	110	12.4
[NTfMs] <sup>-</sup>	TS	158	58	14.0
[NTfMs] <sup>-</sup>	TS	267	93	14.9
[NTfMs] <sup>-</sup>	TS	80	149	17.0
[NTfMs] <sup>-</sup>	TS	353	89	33.2

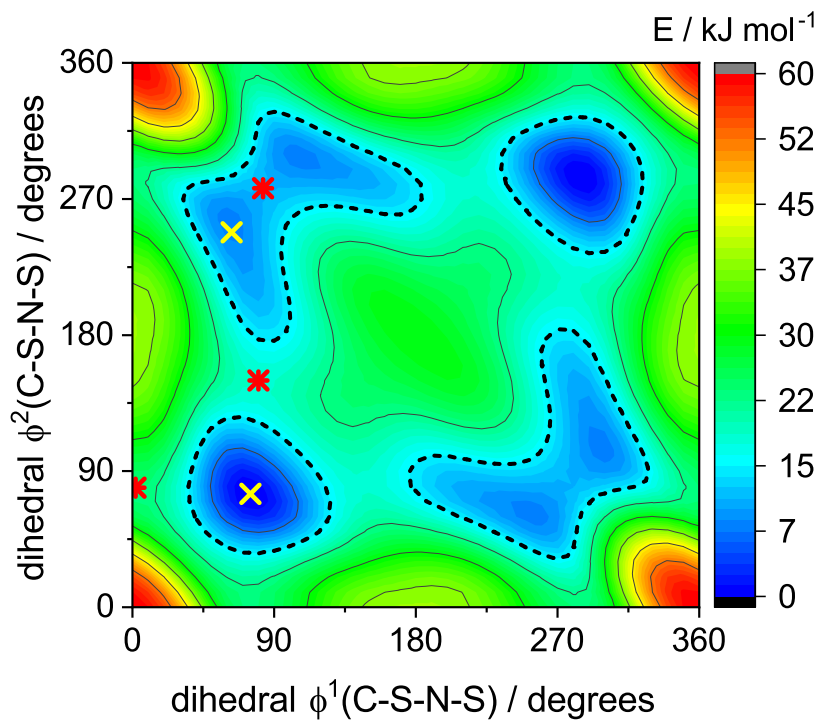


Figure 1: The potential energy surface of the  $[\text{N}(\text{SO}_2\text{CN})_2]^-$  anion. Yellow crosses signs correspond to minimum energy geometries, red stars correspond to transition state geometries.

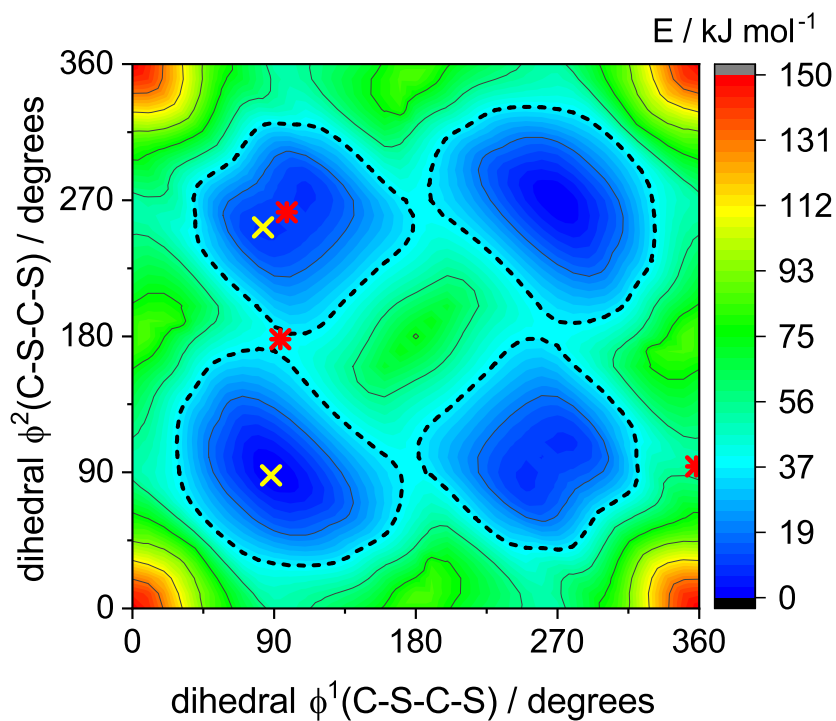


Figure 2: The potential energy surface of the  $[\text{C}(\text{CN})\text{Tf}_2]^-$  anion. Yellow crosses signs correspond to minimum energy geometries, red stars correspond to transition state geometries.

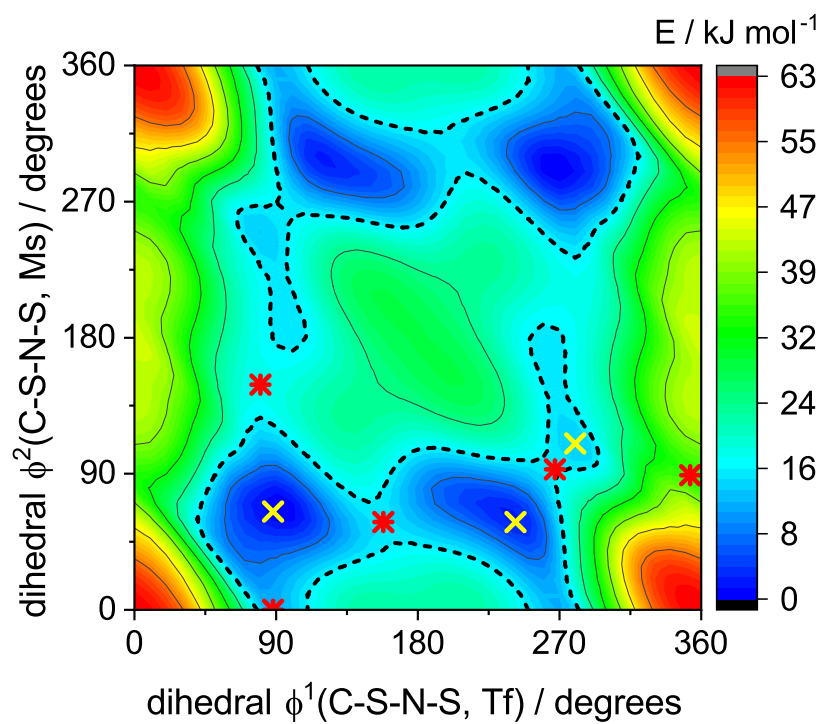


Figure 3: The potential energy surface of the [NTfMs]<sup>-</sup> anion. Yellow crosses signs correspond to minimum energy geometries, red stars correspond to transition state geometries.

## 2 Syntheses

Acetonitrile, tetrahydrofuran, diethyl ether, pentane and toluene were obtained from a pure-Solv 400 solvent purification system (innovative technology, Wanchai, China). In general, solvents were dried and kept dry using MS3Å and MS4Å as appropriate.<sup>1</sup> Water was obtained from an Arium advance EDI Type 2 water purification system (Sartorius, Göttingen, Germany).

Glindemann PTFE sealing rings (SIGMA-ALDRICH, St. Louis, USA) were used with ground glass joints to prevent contamination with grease. Activated charcoal Norit SX ultra, steam activated and acid washed, highly purified (SIGMA-ALDRICH, St. Louis, USA) was used for decolourisation purposes.

Ultrapure glassware was used for the purification steps of  $\text{K}[\text{B}(\text{CN})_4]$  and all steps involved in the synthesis of  $[\text{C}_4\text{C}_{1\text{im}}]\text{Cl}$  (including the purification of starting materials). The cleaning protocol for ultrapure glassware was as follows. Optically clean general purpose glassware was thoroughly rinsed with ethanol or industrial methylated spirits, followed by Decon 90 (Fisher Scientific, Loughborough, United Kingdom) 5% (v/v) in water, and finally deionised water. The glassware was then dried and subsequently rinsed three times with piranha solution ( $\text{H}_2\text{SO}_4:\text{H}_2\text{O}_2$  60:30 by volume), followed by at least four rinses with deionised water, followed by drying in a clean, dedicated oven at 120°C overnight.

The following reagents were used as received: Anhydrous *tert*-butyl alcohol 99.5% (Thermo Fisher Scientific, Ward Hill MA, USA); Trifluoroacetic anhydride 99% (Fluorochem, Hadfield, United Kingdom); Acetic anhydride  $\geq 98\%$  (SLS, Nottingham, United Kingdom); Methanesulfonamide  $> 98.0\%$  (TCI-UK, Oxford, United Kingdom); lithium bis(trifluoromethylsulfonyl)imide 99% (IOLITEC, Heilbronn, Germany); (trimethylsilyl)methyl lithium in hexanes (Fisher Scientific, Loughborough, United Kingdom); Lithium 1,1,2,2,3,3-Hexafluoropropane-1,3-disulfonimide  $> 98.0\%$  (TCI-UK, Oxford, United Kingdom).

Some reagents were purified before use as follows. Distillation and sublimation was performed under Schlenk conditions. Potassium *tert*-butoxide  $\geq 98\%$  (SIGMA-ALDRICH, St. Louis, USA) was sublimed at 200°C; Trifluoromethanesulfonamide 99% (Fluorochem, Hadfield, United Kingdom) was sublimed at 80°C; Methanesulfonyl chloride  $\geq 99\%$  (SIGMA-ALDRICH, St. Louis, USA) was distilled from  $\text{P}_4\text{O}_{10}$ ; Triethylamine  $\geq 99.5\%$  (SIGMA-ALDRICH, St. Louis, USA) was distilled from  $\text{CaH}_2$ ; Trifluoromethanesulfonic anhydride 98% (Fluorochem, Hadfield, United Kingdom) was distilled from  $\text{P}_4\text{O}_{10}$ ; 1-Chlorobutane Reagent-

Plus 99% (SIGMA-ALDRICH, St. Louis, USA) was purified by repeated washes (9 times) with concentrated H<sub>2</sub>SO<sub>4</sub> until the acid phase remained colourless, followed by distillation from P<sub>4</sub>O<sub>10</sub>; 1-Methylimidazole 99% (Fluorochem, Hadfield, United Kingdom) was first stirred with potassium hydroxide overnight, followed by vacuum distillation. The raw methylimidazole thus obtained was further purified by stirring with metallic sodium overnight, followed by vacuum distillation.

Ionic liquids were dried on a Schlenk line with a liquid nitrogen cold trap and an end vacuum of approximately  $5 \cdot 10^{-3}$  mbar / 0.5 Pa. Water content after drying was determined *via* Coulometric Karl Fischer titration using a C20 Compact Karl Fischer Coulometer (Mettler-Toledo, Schwerzenbach, Switzerland). In some cases, the water content of the sample was too low to trigger the Karl Fischer titrator, in these cases the water content was around 30 ppm or less. Testing of washing water and ionic liquids for halides was achieved with 0.3 M AgNO<sub>3</sub> in 1 M HNO<sub>3</sub>. High resolution mass spectra ( $\pm 5$  mDa) were recorded on a LCT Premier mass spectrometer (Waters Corporation, Manchester, United Kingdom). Reported masses do not include the electron/hole in the case of negative/positive ESI. Elemental analysis has been performed on a ThermoFlash 2000 CHN analyser (Thermo Fisher Scientific, Ward Hill MA, USA) using the service provided by London Metropolitan University. Assignment of NMRs has been achieved *via* two dimensional experiments (HMBC, COSY, HSQC) and comparison of coupling constants and chemical shift with known compounds.<sup>2</sup> <sup>11</sup>B NMR were recorded in 5 mm 500 MHz quartz NMR sample tubes (SP Wilmad-LabGlass, Vineland NJ, USA).

The general procedure for ionic liquid metathesis was as follows<sup>3</sup>. To 10 to 20 mmol of a cation precursor ([C<sub>4</sub>C<sub>1</sub>im]Cl) were added 1.15 to 1.20 equivalents of the desired anion precursor (K[B(CN)<sub>4</sub>], Na[CHTf<sub>2</sub>], Li[NTf<sub>2</sub>], *etc*) as well as 20 to 30 mL water and 200 to 300 mL CH<sub>2</sub>Cl<sub>2</sub>. For the syntheses of K[B(CN)<sub>4</sub>] and Na[CHTf<sub>2</sub>] see reference [3]. The resulting mixture was then stirred for an hour, and the organic phase separated. The organic phase was then washed with water (20 to 30 mL each) until no further halide was detected in the washing water using silver nitrate solution. Since Ag[B(CN)<sub>4</sub>] precipitates in water, tetracyanoborate ionic liquids need to be checked for the absence of halides by means of ion chromatography. After removing the CH<sub>2</sub>Cl<sub>2</sub> under reduced pressure using a rotary evaporator, the resulting ionic liquids were dried by stirring under high vacuum at 40°C for several days. After each washing step, the separating funnel was thoroughly rinsed with ethanol and deionised water to avoid transfer of halides.

## 2.1 Precursors

**2.1.1 H[NMs<sub>2</sub>]** Based on Reference [4], see also Reference [5, 6]. 26.34 g NH<sub>4</sub>Cl (492 mmol / 1.00 eq) were dissolved in 125 mL water in a round bottom flask with two dropping funnels. One dropping funnel was charged with 114 g methanesulfonyl chloride (995 mmol / 2.02 eq), and the other dropping funnel was charged with a solution of 79.0 g NaOH (1.98 mol / 4.02 eq) in 200 mL water. The contents of both dropping funnels were added to the ammonium chloride solution simultaneously while cooling in an external ice bath, so that addition was complete after 3 h. After addition was complete, the reaction mixture was stirred for 3 h, and adjusted to pH > 7 by addition of 1.40 g NaOH (35 mmol / 0.07 eq). As much of the solution as feasible was transferred into a Kutscher-Steudel apparatus and continuously washed with CH<sub>2</sub>Cl<sub>2</sub> for 25 h. Then, the collection flask was replaced with a fresh flask with CH<sub>2</sub>Cl<sub>2</sub>, 60 mL concentrated HCl were added to the aqueous phase, and the solution was continuously extracted with CH<sub>2</sub>Cl<sub>2</sub> for 24 h. After removal of the solvent on a rotary evaporator under reduced pressure, 30.8 g raw material were obtained. Further purification was achieved by crystallising twice from glacial acetic acid and drying in high vacuum, which gave 15.6 g bis(methanesulfonyl)amine (68.7 mmol / 14%). <sup>1</sup>H NMR (acetone-d<sub>6</sub>, 400 MHz, δ in ppm): 10.53 (s, 1H, N-H), 3.30 (s, 6H, CH<sub>3</sub>); <sup>13</sup>C{<sup>1</sup>H} NMR (acetone-d<sub>6</sub>, 101 MHz, δ in ppm): 43.09 (s). HRMS, ESI<sup>-</sup>: m/z found 171.9731, calc. 171.9738 (C<sub>2</sub>H<sub>6</sub>NO<sub>4</sub>S<sub>2</sub><sup>-</sup>). Elemental analysis (CHNS): calculated for C<sub>2</sub>H<sub>7</sub>NO<sub>4</sub>S<sub>2</sub>: C, 13.87; H, 4.07; N, 8.09; S, 37.02. Found C, 13.97; H, 4.22; N, 8.01; S, 37.23.

**2.1.2 H[TfNAc]** Based on Reference [7]. 50.4 g TfNH<sub>2</sub> (338 mmol / 1.00 eq) were dissolved in 500 mL dry acetonitrile in a round bottom flask placed in a water bath as heat sink. To the solution were added 100 mL acetic anhydride (1.06 mol / 3.13 eq) and 0.6 mL H<sub>2</sub>SO<sub>4</sub>. After stirring for 15 min, the reaction mixture was slowly heated to 60°C and then stirred at 60°C for 3 h. The reaction mixture was then stirred at ambient temperature overnight, and the solvent removed under reduced pressure using a rotary evaporator. Subsequently, 300 mL toluene were added to the residue. After allowing to crystallise in dry ice for 2.5 h, the solvent was decanted and 200 mL fresh toluene were added. The mixture was briefly stirred at 50°C and allowed to crystallise at 4°C overnight. The process was repeated, *i.e.* after decanting the solvent, 200 mL fresh toluene were added, stirred at 50°C, kept at 4°C overnight, and the solvent decanted again. The resulting solid was washed twice with pentane. To this end, 130 mL (200 mL for the second wash) pentane were added to the solid residue, cooled to dry

ice temperature, and decanted. Remaining pentane was removed by passing dry nitrogen over the raw product, and 40.2 g *N*-((trifluoromethyl)sulfonyl)acetamide (210 mmol / 62%) were obtained by sublimation.  $^1\text{H}$  NMR (MeCN- $\text{d}_3$ , 400 MHz,  $\delta$  in ppm): 10.02 (br s, 1H, N-H), 2.16 (s, 3H, COCH $_3$ );  $^{13}\text{C}\{^1\text{H}\}$  NMR (MeCN- $\text{d}_3$ , 101 MHz,  $\delta$  in ppm): 168.72 (s, COCH $_3$ ), 120.30 (q,  $^1\text{J}_{\text{C/F}} = 320.8$  Hz, SO $_2$ CF $_3$ ), 24.47 (s, COCH $_3$ );  $^{19}\text{F}$  NMR (MeCN- $\text{d}_3$ , 377 MHz,  $\delta$  in ppm): -77.77 (s). HRMS, ESI $^-$ :  $m/z$  found 189.9792, calc. 189.9786 (C $_3$ H $_3$ NO $_3$ F $_3$ S).

**2.1.3 H[NMsTFA]** Based on Reference [7]. 14.7 g MsNH $_2$  (154 mmol / 1.00 eq) were dissolved in 150 mL acetonitrile, and 45 ml trifluoroacetic anhydride (67.3 g / 321 mmol / 2.08 eq) together with 0.27 mL H $_2$ SO $_4$  were added. The reaction mixture was stirred for 13 days at ambient temperature, and the solvent distilled off under reduced pressure at ambient temperature. The residue was washed with 150 mL toluene, cooling in dry ice before decanting, followed by 150 mL toluene, cooled to 4°C before decanting. This was followed by two washes with 100 mL and 50 mL pentane in the same manner, both times cooling in dry ice before decanting. The raw product was dried in high vacuum, followed by sublimation in high vacuum. The sublimation was carried out at a bath temperature of 50°C, which takes several days. Thus, 23.2 g 2,2,2-trifluoro-*N*-(methanesulfonyl)acetamide (121 mmol / 79%) were obtained.  $^1\text{H}$  NMR (MeCN- $\text{d}_3$ , 400 MHz,  $\delta$  in ppm): 10.51 (br s, 1H, N-H), 3.31 (s, 3H, CH $_3$ );  $^{13}\text{C}\{^1\text{H}\}$  NMR (MeCN- $\text{d}_3$ , 101 MHz,  $\delta$  in ppm): 156.79 (q,  $^2\text{J}_{\text{C/F}} = 41.0$  Hz, COCF $_3$ ), 115.76 (q,  $^1\text{J}_{\text{C/F}} = 288.1$  Hz, COCF $_3$ ), 42.03 (s, SO $_2$ CH $_3$ );  $^{19}\text{F}$  NMR (MeCN- $\text{d}_3$ , 377 MHz,  $\delta$  in ppm): -76.29 (s). HRMS, ESI $^-$ :  $m/z$  found 189.9791, calc. 189.9786 (C $_3$ H $_3$ NO $_3$ F $_3$ S).

**2.1.4 H[NTfMs]** 7.24 g [C $_4$ C $_1$ im][NTfMs] were stirred with 1.1 mL H $_2$ SO $_4$ , distilling off a small amount of *N*-(trifluoromethylsulfonyl)methanesulfonamide in high vacuum. The residue was placed in a 25 mL round bottom flask and not moved for 6 months, during which time crystals suitable for X-ray diffraction were deposited on the sides of the flask.  $^1\text{H}$  NMR (MeCN- $\text{d}_3$ , 400 MHz,  $\delta$  in ppm): 9.25-8.97 (m, 1H, N-H), 3.39 (s, 3H, CH $_3$ );  $^{13}\text{C}\{^1\text{H}\}$  NMR (MeCN- $\text{d}_3$ , 101 MHz,  $\delta$  in ppm): 119.90 (q,  $^1\text{J}_{\text{C/F}} = 320.8$  Hz, SO $_2$ CF $_3$ ), 45.10 (s, SO $_2$ CH $_3$ );  $^{19}\text{F}$  NMR (MeCN- $\text{d}_3$ , 377 MHz,  $\delta$  in ppm): -77.57 (s).

**2.1.5 Na[NMsTFA]** 16.1 g H[NMsTFA] (83.6 mmol / 1.00 eq) were stirred with 20 mL water in an ice bath, and slowly neutralised with 7.09 g NaHCO $_3$  (84.4 mmol / 1.01 eq). The resulting solution was freeze dried, and the solid residue dried in high vacuum, giving

18.5 g sodium (methanesulfonyl)(2,2,2-trifluoroacetyl)imide (86.8 mmol / quantitative yield).  $^1\text{H}$  NMR (DMSO- $d_6$ , 400 MHz,  $\delta$  in ppm): 2.82 (s,  $\text{SO}_2\text{CH}_3$ );  $^{13}\text{C}\{^1\text{H}\}$  NMR (DMSO- $d_6$ , 101 MHz,  $\delta$  in ppm): 160.60 (q,  $^2J_{\text{C}/\text{F}} = 33.0$  Hz,  $\text{COCF}_3$ ), 117.48 (q,  $^1J_{\text{C}/\text{F}} = 290.76$  Hz,  $\text{CF}_3$ ), 43.21 (s,  $\text{SO}_2\text{CH}_3$ );  $^{19}\text{F}$  NMR (DMSO- $d_6$ , 377 MHz,  $\delta$  in ppm):  $-74.07$  (s,  $\text{CF}_3$ ).

**2.1.6 Na[TfNAc]** 16.0 g H[TfNAc] (83.6 mmol / 1.00 eq) were stirred with 20 mL water in an ice bath, and slowly neutralised with 7.08 g  $\text{NaHCO}_3$  (84.3 mmol / 1.01 eq). The resulting solution was freeze dried, and the solid residue dried in high vacuum, giving 17.8 g sodium acetyl(trifluoromethylsulfonyl)imide (83.4 mmol / quantitative yield).  $^1\text{H}$  NMR (DMSO- $d_6$ , 400 MHz,  $\delta$  in ppm): 1.82 (s,  $\text{COCH}_3$ );  $^{13}\text{C}\{^1\text{H}\}$  NMR (DMSO- $d_6$ , 101 MHz,  $\delta$  in ppm): 176.21 (s,  $\text{COCH}_3$ ), 120.48 (q,  $^1J_{\text{C}/\text{F}} = 325.1$  Hz,  $\text{CF}_3$ ), 26.91 (s,  $\text{COCH}_3$ );  $^{19}\text{F}$  NMR (DMSO- $d_6$ , 377 MHz,  $\delta$  in ppm):  $-77.84$  (s,  $\text{CF}_3$ ).

**2.1.7 TfNHK** 19.3 g *t*-BuOK (172 mmol / 1.00 eq) dissolved (suspended) in 200 mL dry *t*-BuOH were slowly added to 25.7 g TfNH $_2$  (172 mmol / 1.00 eq) in 100 mL *t*-BuOH with stirring. The mixture was then heated to 85°C for 7 h, and the *t*-BuOH distilled off. After that, the residue was washed with  $\approx 20$  mL dry Et $_2$ O and dried in high vacuum at 55°C overnight, giving 25.5 g potassium ((trifluoromethyl)sulfonyl)amide (136 mmol / 79%).  $^1\text{H}$  NMR (DMSO- $d_6$ , 400 MHz,  $\delta$  in ppm): 2.60 (s, NH);  $^{13}\text{C}\{^1\text{H}\}$  NMR (DMSO- $d_6$ , 101 MHz,  $\delta$  in ppm): 122.34 (q,  $^1J_{\text{C}/\text{F}} = 329.7$  Hz,  $\text{CF}_3$ );  $^{19}\text{F}$  NMR (DMSO- $d_6$ , 377 MHz,  $\delta$  in ppm):  $-78.65$  (s,  $\text{CF}_3$ ).

**2.1.8 Li[NTfMs]** Based on Reference [8]. 25.2 g TfNHK (135 mmol / 1.01 eq), 13.5 g triethyl amine (133 mmol / 1.00 eq) and 200 mL acetonitrile were added together in a 500 mL round bottom flask in the glovebox and heated to 50°C. Then, 15.7 g methanesulfonyl chloride (137 mmol / 1.02 eq) were added dropwise over 15 min, and the reaction mixture heated to reflux for 48 h. The solids were filtered off, and the solvent removed from the filtrate by distillation under reduced pressure. Then, 5.48 g lithium hydroxide monohydrate (130 mmol / 0.98 eq) dissolved in 50 mL water were added to the residue and stirred until homogeneous. The water was removed again by distillation under reduced pressure, a small amount of activated carbon added to the residue, and the solids were extracted twice with 50 mL acetonitrile each. The combined organic phases were filtered through filter paper, followed by filtration through a 0.3  $\mu\text{m}$  syringe filter, and the bulk amount of acetonitrile removed by distillation under reduced

pressure. The residue was then ground with toluene followed by pentane, and dried in high vacuum. Thus, 28.1 g lithium (methylsulfonyl)((trifluoromethyl)sulfonyl)amide (120 mmol / 89%) were obtained.  $^1\text{H}$  NMR (DMSO- $d_6$ , 400 MHz,  $\delta$  in ppm): 2.85 (s, 3H,  $\text{SO}_2\text{CH}_3$ );  $^{13}\text{C}\{^1\text{H}\}$  NMR (DMSO- $d_6$ , 101 MHz,  $\delta$  in ppm): 120.42 (q,  $^1J_{\text{C/F}} = 324.3$  Hz,  $\text{SO}_2\text{CF}_3$ ), 43.26 (s,  $\text{SO}_2\text{CH}_3$ );  $^{19}\text{F}$  NMR (DMSO- $d_6$ , 377 MHz,  $\delta$  in ppm): -77.58 (s). HRMS, ESI $^-$ :  $m/z$  found 225.9447, calc. 225.9456 ( $\text{C}_2\text{H}_3\text{NO}_4\text{S}_2\text{F}_3^-$ ).

**2.1.9 [C<sub>4</sub>C<sub>1</sub>im]Cl** To 220 mL (227 g / 2.77 mol / 1.00 eq) methylimidazole magnetically stirred at 0°C were added 200 mL ethyl acetate followed by 330 mL (291 g / 3.14 mol / 1.13 eq) chlorobutane. The reaction mixture was then allowed to warm to 20°C overnight and stirred for seven days. Subsequently, the temperature of the reaction mixture was increased stepwise in increments of 10°C every seven days, reaching 50°C after three weeks, and then kept at 50°C for 20 days. Then, the reaction mixture was cooled to 4°C and allowed to crystallise without stirring for two days. The solvent was decanted from the crystals, and 150 mL fresh ethyl acetate were added. After melting the solids at 70°C, the mixture was again allowed to crystallise at 4°C for two days. The solvent was again decanted and replaced by 150 mL fresh ethyl acetate, the solids melted by heating to 77°C, and allowed to crystallise at ambient temperature overnight. After decanting the solvent and washing with fresh ethyl acetate, the crude product was crystallised twice from a mixture of 50 mL acetonitrile and 200 mL ethyl acetate, and then a third time from a mixture of 100 mL acetonitrile and 300 mL ethyl acetate. The last crystallisation required a seed crystal. The pure product was then obtained by drying in high vacuum for several days, and stored in a glovebox.  $^1\text{H}$  NMR (DMSO- $d_6$ , 400 MHz,  $\delta$  in ppm): 9.61 (s, 1H, N-CH-N), 7.91 (s, 1H, HC=CH), 7.83 (s, 1H, HC=CH), 4.20 (t,  $^3J_{\text{H/H}} = 7.2$  Hz, 2H, N-CH<sub>2</sub>), 3.88 (s, 3H, N-CH<sub>3</sub>), 1.75 (p,  $^3J_{\text{H/H}} = 7.3$  Hz, 2H, N-CH<sub>2</sub>-CH<sub>2</sub>), 1.23 (h,  $^3J_{\text{H/H}} = 7.4$  Hz, 2H, CH<sub>2</sub>-CH<sub>3</sub>), 0.87 (t,  $^3J_{\text{H/H}} = 7.4$  Hz, 3H, CH<sub>2</sub>-CH<sub>3</sub>);  $^{13}\text{C}\{^1\text{H}\}$  NMR (DMSO- $d_6$ , 101 MHz,  $\delta$  in ppm): 136.75 (s, N-CH-N), 123.53 (s, HC=CH), 122.25 (s, HC=CH), 48.33 (s, N-CH<sub>2</sub>), 35.66 (s, N-CH<sub>3</sub>), 31.38 (s, N-CH<sub>2</sub>-CH<sub>2</sub>), 18.74 (s, CH<sub>2</sub>-CH<sub>3</sub>), 13.27 (s, CH<sub>2</sub>-CH<sub>3</sub>). Elemental analysis (CHN): calculated for C<sub>10</sub>H<sub>21</sub>N<sub>3</sub>O<sub>4</sub>S<sub>2</sub>: C, 55.01; H, 8.66; N, 16.04; Found C, 53.69; H, 9.14; N, 15.35.

**2.1.10 [N1111][NMs<sub>2</sub>]** 0.5378 g H[NMs<sub>2</sub>] were dissolved in 3 mL methanol and neutralised with 1.308 mL tetramethylammonium hydroxide 25% in methanol. The solvent was removed under reduced pressure, and crystals grown by slow evaporation after redissolving the residue

in methylene chloride. Crystals of [N1111][NMsTFA] and [N1111][NTfAc] were obtained accordingly from the respective free acids.

## 2.2 Ionic Liquids

**2.2.1 [C<sub>4</sub>C<sub>1</sub>im][6cPFSI]** 5.10 g [C<sub>4</sub>C<sub>1</sub>im]Cl (29.2 mmol / 1.00 eq) and 10.5 g Li[6cPFSI] (35.0 mmol / 1.20 eq) were converted to 12.5 g 1-butyl-3-methylimidazolium 1,1,2,2,3,3-Hexafluoropropane-1,3-disulfonimide (28.9 mmol / 99%) using the general procedure, washing the CH<sub>2</sub>Cl<sub>2</sub> phase thrice with water. Water content after drying was below detection limit. <sup>1</sup>H NMR (DMSO-d<sub>6</sub>, 400 MHz, δ in ppm): 9.10 (s, 1H, N-**CH**-N), 7.75-7.73 (m, 1H, **HC**=CH), 7.69-7.66 (m, 1H, HC=**CH**), 4.16 (t, <sup>3</sup>J<sub>H/H</sub> = 7.2 Hz, 2H, N-**CH**<sub>2</sub>), 3.85 (s, 3H, N-**CH**<sub>3</sub>), 1.77 (p, <sup>3</sup>J<sub>H/H</sub> = 7.46 Hz, 2H, N-CH<sub>2</sub>-**CH**<sub>2</sub>), 1.27 (h, <sup>3</sup>J<sub>H/H</sub> = 7.4 Hz, 2H, **CH**<sub>2</sub>-CH<sub>3</sub>), 0.90 (t, <sup>3</sup>J<sub>H/H</sub> = 7.4 Hz, 3H, CH<sub>2</sub>-**CH**<sub>3</sub>); <sup>13</sup>C{<sup>1</sup>H} NMR (DMSO-d<sub>6</sub>, 101 MHz, δ in ppm): 136.52 (s, N-**CH**-N), 123.61 (s, **HC**=CH), 122.24 (s, HC=**CH**), 112.43 (tt, <sup>1</sup>J<sub>C/F</sub> = 297.4 Hz, <sup>2</sup>J<sub>C/F</sub> 25.1 Hz, SO<sub>2</sub>**CF**<sub>2</sub>), 109.35 (tp, <sup>1</sup>J<sub>C/F</sub> = 273.5 Hz, <sup>2</sup>J<sub>C/F</sub> 26.0 Hz, CF<sub>2</sub>-**CF**<sub>2</sub>-CF<sub>2</sub>), 48.56 (s, N-**CH**<sub>2</sub>), 35.71 (s, N-**CH**<sub>3</sub>), 31.37 (s, N-CH<sub>2</sub>-**CH**<sub>2</sub>), 18.77 (s, **CH**<sub>2</sub>-CH<sub>3</sub>), 13.16 (s, CH<sub>2</sub>-**CH**<sub>3</sub>); <sup>19</sup>F NMR (DMSO-d<sub>6</sub>, 377 MHz, δ in ppm): -119.69 (s, SO<sub>2</sub>**CF**<sub>2</sub>), -125.98 (s, CF<sub>2</sub>-**CF**<sub>2</sub>-CF<sub>2</sub>). HRMS, ESI<sup>+</sup>: m/z found 139.1242, calc. 139.1235 (C<sub>8</sub>H<sub>15</sub>N<sub>2</sub><sup>+</sup>); ESI<sup>-</sup>: m/z found 291.9180, calc. 291.9173 (C<sub>3</sub>NO<sub>4</sub>S<sub>2</sub>F<sub>6</sub><sup>-</sup>).

**2.2.2 [C<sub>4</sub>C<sub>1</sub>im][NTf<sub>2</sub>]** 42.2 g [C<sub>4</sub>C<sub>1</sub>im]Cl (241 mmol / 1.00 eq) and 81.2 g Li[NTf<sub>2</sub>] (283 mmol / 1.17 eq) were converted to 99.7 g [P444(2O2)][NTf<sub>2</sub>] (238 mmol / 98%) using the general procedure, washing the CH<sub>2</sub>Cl<sub>2</sub> phase thrice with water. Water content after drying was 25 ppm. <sup>1</sup>H NMR (DMSO-d<sub>6</sub>, 400 MHz, δ in ppm): 9.10 (s, 1H, N-**CH**-N), 7.75 (s, 1H, **HC**=CH), 7.68 (s, 1H, HC=**CH**), 4.16 (t, <sup>3</sup>J<sub>H/H</sub> = 7.2 Hz, 2H, N-**CH**<sub>2</sub>), 3.85 (s, 3H, N-**CH**<sub>3</sub>), 1.77 (tt, <sup>3</sup>J<sub>H/H</sub> = 9.0 Hz, <sup>3</sup>J<sub>H/H</sub> = 6.8 Hz, 2H, N-CH<sub>2</sub>-**CH**<sub>2</sub>), 1.28 (h, <sup>3</sup>J<sub>H/H</sub> = 7.4 Hz, 2H, **CH**<sub>2</sub>-CH<sub>3</sub>), 0.90 (t, <sup>3</sup>J<sub>H/H</sub> = 7.4 Hz, 3H, CH<sub>2</sub>-**CH**<sub>3</sub>); <sup>13</sup>C{<sup>1</sup>H} NMR (DMSO-d<sub>6</sub>, 101 MHz, δ in ppm): 138.14 (s, N-**CH**-N), 124.07 (s, **HC**=CH), 122.72 (s, HC=**CH**), 119.97 (q, <sup>1</sup>J<sub>C/F</sub> = 322.1 Hz, **CF**<sub>3</sub>), 48.39 (s, N-**CH**<sub>2</sub>), 35.53 (s, N-**CH**<sub>3</sub>), 32.23 (s, N-CH<sub>2</sub>-**CH**<sub>2</sub>), 20.08 (s, **CH**<sub>2</sub>-CH<sub>3</sub>), 12.68 (s, CH<sub>2</sub>-**CH**<sub>3</sub>); <sup>19</sup>F NMR (DMSO-d<sub>6</sub>, 377 MHz, δ in ppm): -78.75 (s). HRMS, ESI<sup>+</sup>: m/z found 139.1236, calc. 139.1235 (C<sub>8</sub>H<sub>15</sub>N<sub>2</sub><sup>+</sup>); ESI<sup>-</sup>: m/z found 279.9182, calc. 279.9173 (C<sub>2</sub>NO<sub>4</sub>F<sub>6</sub>S<sub>2</sub><sup>-</sup>).

**2.2.3** [C<sub>4</sub>C<sub>1</sub>im][NMs<sub>2</sub>] Based on Reference [9]. A column with glass frit was filled with strongly basic anion exchange resin (AmberLite IRN78 OH). The resin was rinsed slowly with 2 L of NaOH 5% (w/v) in water, then with water so that the eluent was neutral and halide free. Then, 5.06 g [C<sub>4</sub>C<sub>1</sub>im]Cl (29.0 mmol) dissolved in 150 mL water were slowly passed over the column over the course of 24 h. After collecting 200 mL eluent with pH ≤ 7, a fraction with a volume of 500 mL and pH ≥ 7 was collected. To this fraction, HNMs<sub>2</sub> was slowly added until the solution was neutral (Monitoring with a pH meter). Removal of the water under reduced pressure using a rotary evaporator (bath temperature 20°C) and drying in high vacuum gave 8.79 g [C<sub>4</sub>C<sub>1</sub>im][NMs<sub>2</sub>] (28.2 mmol / 97%). Water content after drying was 69 ppm. The partition coefficient D<sub>2</sub>O/CD<sub>2</sub>Cl<sub>2</sub> was approximately 8, as estimated by NMR. <sup>1</sup>H NMR (DMSO-d<sub>6</sub>, 400 MHz, δ in ppm): 9.14 (s, 1H, N-CH-N), 7.81-7.74 (m, 1H, HC=CH), 7.73-7.67 (m, 1H, HC=CH), 4.17 (t, <sup>3</sup>J<sub>H/H</sub> = 7.2 Hz, 2H, N-CH<sub>2</sub>), 3.86 (s, 3H, N-CH<sub>3</sub>), 2.74 (s, 6H, SO<sub>2</sub>CH<sub>3</sub>), 1.76 (p, <sup>3</sup>J<sub>H/H</sub> = 7.4 Hz, 2H, N-CH<sub>2</sub>-CH<sub>2</sub>), 1.28 (h, <sup>3</sup>J<sub>H/H</sub> = 7.4 Hz, 2H, CH<sub>2</sub>-CH<sub>3</sub>), 0.90 (t, <sup>3</sup>J<sub>H/H</sub> = 7.4 Hz, 3H, CH<sub>2</sub>-CH<sub>3</sub>); <sup>13</sup>C{<sup>1</sup>H} NMR (DMSO-d<sub>6</sub>, 101 MHz, δ in ppm): 136.54 (s, N-CH-N), 123.63 (s, HC=CH), 122.26 (s, HC=CH), 48.49 (s, N-CH<sub>2</sub>), 42.16 (s, SO<sub>2</sub>CH<sub>3</sub>), 35.76 (s, N-CH<sub>3</sub>), 31.38 (s, N-CH<sub>2</sub>-CH<sub>2</sub>), 18.79 (s, CH<sub>2</sub>-CH<sub>3</sub>), 13.30 (s, CH<sub>2</sub>-CH<sub>3</sub>). HRMS, ESI<sup>+</sup>: m/z found 139.1228, calc. 139.1235 (C<sub>8</sub>H<sub>15</sub>N<sub>2</sub><sup>+</sup>); ESI<sup>-</sup>: m/z found 171.9740, calc. 171.9738 (C<sub>2</sub>H<sub>6</sub>NO<sub>4</sub>S<sub>2</sub><sup>-</sup>). Elemental analysis (CHNS): calculated for C<sub>10</sub>H<sub>21</sub>N<sub>3</sub>O<sub>4</sub>S<sub>2</sub>: C, 38.57; H, 6.80; N, 13.49; S, 20.59. Found C, 37.30; H, 6.43; N, 14.64; S, 20.74. Elemental analysis (CHN): calculated for C<sub>10</sub>H<sub>21</sub>N<sub>3</sub>O<sub>4</sub>S<sub>2</sub>: C, 38.57; H, 6.80; N, 13.49; Found C, 39.14; H, 7.00; N, 13.36.

**2.2.4** [C<sub>4</sub>C<sub>1</sub>im][B(CN)<sub>4</sub>] 11.1 g [C<sub>4</sub>C<sub>1</sub>im]Cl (63.5 mmol / 1.00 eq) and 11.7 g K[B(CN)<sub>4</sub>] (76.2 mmol / 1.20 eq) were converted to 15.4 g 1-butyl-3-methylimidazolium tetracyanoborate (60.6 mmol / 95%) using the general procedure, washing the CH<sub>2</sub>Cl<sub>2</sub> phase 10 times with water. Water content after drying was 62 ppm. <sup>1</sup>H NMR (DMSO-d<sub>6</sub>, 400 MHz, δ in ppm): 9.10 (s, 1H, N-CH-N), 7.76-7.71 (s, 1H, HC=CH), 7.70-7.64 (s, 1H, HC=CH), 4.16 (t, <sup>3</sup>J<sub>H/H</sub> = 7.2 Hz, 2H, N-CH<sub>2</sub>), 3.84 (s, 3H, N-CH<sub>3</sub>), 1.83-1.70 (m, 2H, N-CH<sub>2</sub>-CH<sub>2</sub>), 1.27 (h, <sup>3</sup>J<sub>H/H</sub> = 7.5 Hz, 2H, CH<sub>2</sub>-CH<sub>3</sub>), 0.91 (t, <sup>3</sup>J<sub>H/H</sub> = 7.4 Hz, 3H, CH<sub>2</sub>-CH<sub>3</sub>); <sup>13</sup>C{<sup>1</sup>H} NMR (DMSO-d<sub>6</sub>, 101 MHz, δ in ppm): 136.48 (s, N-CH-N), 123.56 (s, HC=CH), 122.20 (s, HC=CH), 121.73 (q, <sup>1</sup>J<sub>C/B</sub> = 70.7 Hz, <sup>11</sup>B-CN), 121.63 (sep, <sup>1</sup>J<sub>C/B</sub> = 23.4 Hz, <sup>1</sup>B-CN), 48.53 (s, N-CH<sub>2</sub>), 35.69 (s, N-CH<sub>3</sub>), 31.33 (s, N-CH<sub>2</sub>-CH<sub>2</sub>), 18.75 (s, CH<sub>2</sub>-CH<sub>3</sub>), 13.15 (s, CH<sub>2</sub>-CH<sub>3</sub>); <sup>11</sup>B

NMR (DMSO- $d_6$ , 128 MHz,  $\delta$  in ppm):  $-38.54$  (s). HRMS, ESI<sup>+</sup>:  $m/z$  found 139.1225, calc. 139.1235 (C<sub>8</sub>H<sub>15</sub>N<sub>2</sub><sup>+</sup>); ESI<sup>-</sup>:  $m/z$  found 115.0221, calc. 115.0216 (<sup>11</sup>BC<sub>4</sub>N<sub>4</sub><sup>-</sup>). Elemental analysis (CHNS): calculated for C<sub>12</sub>H<sub>15</sub>BN<sub>6</sub>: C, 56.72; H, 5.95; N, 33.07; S, 0.00. Found C, 56.33; H, 5.82; N, 33.69; S, 0.00.

**2.2.5 [C<sub>4</sub>C<sub>1</sub>im][CHTf<sub>2</sub>]** First, a solution of Na[CHTf<sub>2</sub>] was prepared. To this end, 20.6 g CH<sub>2</sub>Tf<sub>2</sub> (73.4 mmol / 1.21 eq) were suspended in 40 mL cold water in an external ice bath. Then, 6.14 g NaHCO<sub>3</sub> (73.1 mmol / 1.20 eq) were slowly added with stirring. Occasionally the reaction vessel was briefly sonicated and the headspace purged with N<sub>2</sub> to liberate CO<sub>2</sub>. The solution was stirred with a small amount of activated carbon, which was removed again by filtering through a 0.2  $\mu$ m syringe filter, washing the filter and residues with  $\approx$  5 mL water. To the resulting clear, homogeneous, neutral solution were added 10.6 g [C<sub>4</sub>C<sub>1</sub>im]Cl (60.9 mmol / 1.00 eq) and 300 mL CH<sub>2</sub>Cl<sub>2</sub>. The mixture was stirred for 1 h, and the phases separated. The organic phase was washed thrice with 20 mL water each, dried over MS4Å, and the solvent removed under reduced pressure using a rotary evaporator. The remaining liquid was dried in high vacuum, giving 22.7 g [C<sub>4</sub>C<sub>1</sub>im][CHTf<sub>2</sub>] (54.3 mmol / 89%). Water content after drying was 46 ppm. <sup>1</sup>H NMR (DMSO- $d_6$ , 400 MHz,  $\delta$  in ppm): 9.08 (s, 1H, N-CH-N), 7.75-7.70 (m, 1H, HC=CH), 7.67-7.64 (m, 1H, HC=CH), 4.16 (t, <sup>3</sup>J<sub>H/H</sub> = 7.2 Hz, 2H, N-CH<sub>2</sub>), 3.92 (s, 1H, CF<sub>3</sub>), 3.85 (s, 3H, N-CH<sub>3</sub>), 1.78 (p, <sup>3</sup>J<sub>H/H</sub> = 7.5 Hz, 2H, N-CH<sub>2</sub>-CH<sub>2</sub>), 1.28 (h, <sup>3</sup>J<sub>H/H</sub> = 7.4 Hz, 2H, CH<sub>2</sub>-CH<sub>3</sub>), 0.91 (t, <sup>3</sup>J<sub>H/H</sub> = 7.4 Hz, 3H, CH<sub>2</sub>-CH<sub>3</sub>); <sup>13</sup>C{<sup>1</sup>H} NMR (DMSO- $d_6$ , 101 MHz,  $\delta$  in ppm): 136.50 (s, N-CH-N), 123.57 (s, HC=CH), 122.22 (s, HC=CH), 120.79 (q, <sup>1</sup>J<sub>C/F</sub> = 326.0 Hz, CF<sub>3</sub>), 53.92 (hept, <sup>3</sup>J<sub>C/F</sub> = 2.7 Hz, CHTf<sub>2</sub>), 48.59 (s, N-CH<sub>2</sub>), 35.64 (s, N-CH<sub>3</sub>), 31.36 (s, N-CH<sub>2</sub>-CH<sub>2</sub>), 18.74 (s, CH<sub>2</sub>-CH<sub>3</sub>), 13.04 (s, CH<sub>2</sub>-CH<sub>3</sub>); <sup>19</sup>F NMR (CDCl<sub>3</sub>, 377 MHz,  $\delta$  in ppm):  $-80.92$  (s). HRMS, ESI<sup>+</sup>:  $m/z$  found 139.1229, calc. 139.1235 (C<sub>8</sub>H<sub>15</sub>N<sub>2</sub><sup>+</sup>); ESI<sup>-</sup>:  $m/z$  found 278.9223, calc. 278.9220 (C<sub>3</sub>HO<sub>4</sub>S<sub>2</sub>F<sub>6</sub><sup>-</sup>).

**2.2.6 [C<sub>4</sub>C<sub>1</sub>im][NTfAc]** First, a solution of Na[NTfAc] was prepared. To this end, 23.4 g H[NTfAc] (123 mmol / 1.21 eq) were suspended in 40 mL cold water in an external ice bath. Then, 10.3 g NaHCO<sub>3</sub> (123 mmol / 1.21 eq) were slowly added with stirring. Occasionally the reaction vessel was briefly sonicated and the headspace purged with N<sub>2</sub> to liberate CO<sub>2</sub>. To the resulting clear, homogeneous, neutral solution were added 17.7 g [C<sub>4</sub>C<sub>1</sub>im]Cl (101 mmol / 1.00 eq) and 300 mL CH<sub>2</sub>Cl<sub>2</sub>. The mixture was stirred for 1 h, and the phases separated. The organic phase was washed thrice with 20 mL water each, dried over MS4Å, and the solvent

removed under reduced pressure using a rotary evaporator. The remaining liquid was dried in high vacuum, giving 27.8 g [C<sub>4</sub>C<sub>1</sub>im][NTfAc] (84.5 mmol / 83%). Water content after drying was 46 ppm. <sup>1</sup>H NMR (DMSO-d<sub>6</sub>, 400 MHz, δ in ppm): 9.14 (s, 1H, N-CH-N), 7.79-7.75 (m, 1H, HC=CH), 7.72-7.68 (m, 1H, HC=CH), 4.17 (t, <sup>3</sup>J<sub>H/H</sub> = 7.2 Hz, 2H, N-CH<sub>2</sub>), 3.86 (s, 3H, N-CH<sub>3</sub>), 1.82 (s, 3H, COCH<sub>3</sub>), 1.81-1.71 (m, 2H, N-CH<sub>2</sub>-CH<sub>2</sub>), 1.26 (h, <sup>3</sup>J<sub>H/H</sub> = 7.4 Hz, 2H, CH<sub>2</sub>-CH<sub>3</sub>), 0.89 (t, <sup>3</sup>J<sub>H/H</sub> = 7.4 Hz, 3H, CH<sub>2</sub>-CH<sub>3</sub>); <sup>13</sup>C{<sup>1</sup>H} NMR (DMSO-d<sub>6</sub>, 101 MHz, δ in ppm): 175.68 (s, COCH<sub>3</sub>), 136.62 (s, N-CH-N), 123.61 (s, HC=CH), 122.27 (s, HC=CH), 120.50 (q, <sup>1</sup>J<sub>C/F</sub> = 325.3 Hz, SO<sub>2</sub>CF<sub>3</sub>), 48.52 (s, N-CH<sub>2</sub>), 35.66 (s, N-CH<sub>3</sub>), 31.40 (s, N-CH<sub>2</sub>-CH<sub>2</sub>), 26.72 (s, COCH<sub>3</sub>), 18.76 (s, CH<sub>2</sub>-CH<sub>3</sub>), 13.14 (s, CH<sub>2</sub>-CH<sub>3</sub>); <sup>19</sup>F NMR (DMSO-d<sub>6</sub>, 377 MHz, δ in ppm): -77.77 (s). HRMS, ESI<sup>+</sup>: m/z found 139.1229, calc. 139.1235 (C<sub>8</sub>H<sub>15</sub>N<sub>2</sub><sup>+</sup>); ESI<sup>-</sup>: m/z found 189.9783, calc. 189.9786 (C<sub>3</sub>H<sub>3</sub>NO<sub>3</sub>F<sub>3</sub>S<sup>-</sup>).

**2.2.7 [C<sub>4</sub>C<sub>1</sub>im][NTfMs]** 3.59 g [C<sub>4</sub>C<sub>1</sub>im]Cl (20.6 mmol / 1.00 eq) and 5.90 g Li[NTfMs] (25.3 mmol / 1.23 eq) were converted to 6.61 g 1-butyl-3-methylimidazolium (methylsulfonyl)-((trifluoromethyl)sulfonyl)amide (18.1 mmol / 88%) using the general procedure, washing the CH<sub>2</sub>Cl<sub>2</sub> phase twice with water. Water content after drying was below detection limit. <sup>1</sup>H NMR (DMSO-d<sub>6</sub>, 400 MHz, δ in ppm): 9.09 (s, 1H, N-CH-N), 7.77-7.74 (m, 1H, HC=CH), 7.70-7.67 (m, 1H, HC=CH), 4.16 (t, <sup>3</sup>J<sub>H/H</sub> = 7.2 Hz, 2H, N-CH<sub>2</sub>), 3.85 (s, 3H, N-CH<sub>3</sub>), 2.87 (s, 3H, SO<sub>2</sub>CH<sub>3</sub>), 1.77 (p, <sup>3</sup>J<sub>H/H</sub> = 7.5 Hz, 2H, N-CH<sub>2</sub>-CH<sub>2</sub>), 1.26 (h, <sup>3</sup>J<sub>H/H</sub> = 7.3 Hz, 2H, CH<sub>2</sub>-CH<sub>3</sub>), 0.90 (t, <sup>3</sup>J<sub>H/H</sub> = 7.4 Hz, 3H, CH<sub>2</sub>-CH<sub>3</sub>); <sup>13</sup>C{<sup>1</sup>H} NMR (DMSO-d<sub>6</sub>, 101 MHz, δ in ppm): 136.94 (s, N-CH-N), 124.06 (s, HC=CH), 122.71 (s, HC=CH), 120.62 (q, <sup>1</sup>J<sub>C/F</sub> = 324.3 Hz, SO<sub>2</sub>CF<sub>3</sub>), 48.97 (s, N-CH<sub>2</sub>), 43.38 (s, SO<sub>2</sub>CH<sub>3</sub>), 36.19 (s, N-CH<sub>3</sub>), 31.81 (s, N-CH<sub>2</sub>-CH<sub>2</sub>), 19.22 (s, CH<sub>2</sub>-CH<sub>3</sub>), 13.69 (s, CH<sub>2</sub>-CH<sub>3</sub>); <sup>19</sup>F NMR (DMSO-d<sub>6</sub>, 377 MHz, δ in ppm): -77.60 (s). HRMS, ESI<sup>+</sup>: m/z found 139.1230, calc. 139.1235 (C<sub>8</sub>H<sub>15</sub>N<sub>2</sub><sup>+</sup>); ESI<sup>-</sup>: m/z found 225.9451, calc. 225.9456 (C<sub>2</sub>H<sub>3</sub>NO<sub>4</sub>F<sub>3</sub>S<sub>2</sub><sup>-</sup>).

**2.2.8 [C<sub>4</sub>C<sub>1</sub>im][NMSTFA]** First, a solution of Na[NMSTFA] was prepared. To this end, 23.2 g H[NMSTFA] (121 mmol / 1.23 eq) were suspended in 30 mL cold water in an external ice bath. Then, 10.2 g NaHCO<sub>3</sub> (121 mmol / 1.23 eq) were slowly added with stirring. Occasionally the reaction vessel was briefly sonicated and the headspace purged with N<sub>2</sub> to liberate CO<sub>2</sub>. To the resulting clear, homogeneous, neutral solution were added 17.2 g [C<sub>4</sub>C<sub>1</sub>im]Cl (98.6 mmol / 1.00 eq) and 300 mL CH<sub>2</sub>Cl<sub>2</sub>. The mixture was stirred for 1 h, and the phases separated. The organic phase was washed thrice with 20 mL water each, dried over MS4Å, and the solvent

removed under reduced pressure using a rotary evaporator. The remaining liquid was dried in high vacuum, giving 22.0 g [C<sub>4</sub>C<sub>1</sub>im][NMsTFA] (66.8 mmol / 68%). Water content after drying was 33 ppm. <sup>1</sup>H NMR (DMSO-d<sub>6</sub>, 400 MHz, δ in ppm): 9.11 (s, 1H, N-**CH**-N), 7.77 (s, 1H, **HC=CH**), 7.70 (s, 1H, HC=**CH**), 4.17 (t, <sup>3</sup>J<sub>H/H</sub> = 7.2 Hz, 2H, N-**CH**<sub>2</sub>), 3.86 (s, 3H, N-**CH**<sub>3</sub>), 2.84 (s, 3H, SO<sub>2</sub>**CH**<sub>3</sub>), 1.76 (p, <sup>3</sup>J<sub>H/H</sub> = 7.3 Hz, 2H, N-CH<sub>2</sub>-**CH**<sub>2</sub>), 1.25 (h, <sup>3</sup>J<sub>H/H</sub> = 7.4 Hz, 2H, **CH**<sub>2</sub>-CH<sub>3</sub>), 0.89 (t, <sup>3</sup>J<sub>H/H</sub> = 7.4 Hz, 3H, CH<sub>2</sub>-**CH**<sub>3</sub>); <sup>13</sup>C{<sup>1</sup>H} NMR (DMSO-d<sub>6</sub>, 101 MHz, δ in ppm): 160.34 (q, <sup>2</sup>J<sub>C/F</sub> = 33.0 Hz, **COCF**<sub>3</sub>), 136.55 (s, N-**CH**-N), 123.60 (s, **HC=CH**), 122.27 (s, HC=**CH**), 117.40 (q, <sup>1</sup>J<sub>C/F</sub> = 291.0 Hz, **COCF**<sub>3</sub>), 48.52 (s, N-**CH**<sub>2</sub>), 39.95 (s, SO<sub>2</sub>**CH**<sub>3</sub>), 35.68 (s, N-**CH**<sub>3</sub>), 31.38 (s, N-CH<sub>2</sub>-**CH**<sub>2</sub>), 18.75 (s, **CH**<sub>2</sub>-CH<sub>3</sub>), 13.14 (s, CH<sub>2</sub>-**CH**<sub>3</sub>); <sup>19</sup>F NMR (DMSO-d<sub>6</sub>, 377 MHz, δ in ppm): -74.17 (s). HRMS, ESI<sup>+</sup>: m/z found 139.1230, calc. 139.1235 (C<sub>8</sub>H<sub>15</sub>N<sub>2</sub><sup>+</sup>); ESI<sup>-</sup>: m/z found 189.9794, calc. 189.9786 (C<sub>3</sub>H<sub>3</sub>NO<sub>3</sub>F<sub>3</sub>S<sup>-</sup>).

### 3 Single Crystal XRD

Crystals were obtained as described above. Datasets were collected using an Oxford Diffraction Xcalibur 3E (Mo Kα radiation, 0.71073 Å). Data processing was carried out using CrysAlisPro,<sup>10</sup> solutions were solved and refined using Olex-2.<sup>11</sup> Hydrogen atoms were placed in geometrically assigned positions with X-H distances of 0.86 Å (NH), 0.95 Å (CH), 0.97 Å (CH<sub>2</sub>) or 0.98 Å (CH<sub>3</sub>) and refined using a riding model, with U<sub>iso</sub>(H) = 1.2 U<sub>eq</sub>(C) (CH, CH<sub>2</sub>), 1.5 U<sub>eq</sub>(C) (CH<sub>3</sub>) or 1.2 U<sub>eq</sub>(N) (NH). Graphics were generated using Olex-2 and Mercury.<sup>12</sup> CCDC reference numbers 1871441 (H[NMs<sub>2</sub>]), 1871442 ([N<sub>1111</sub>][NMs<sub>2</sub>]), 1871443 (Li[NTfMs]), 1871444 (H[NTfMs]), and 1871445 ([C<sub>4</sub>C<sub>1</sub>im][NMs<sub>2</sub>]) contain crystallographic data in CIF format, which is also summarized below (Table 12). [C<sub>4</sub>C<sub>1</sub>im][NMs<sub>2</sub>] was refined as a 2-component twin with BASF 0.251(2).

Single crystal XRD results are summarised in Table 2. Five new crystal structures containing the novel anions in this work could be obtained, additional relevant crystallographic data is provided in Reference [13]. The two backbone dihedral angles were read from the refined structures, and are listed in Table 3 together with the backbone dihedral angles predicted from *ab initio* simulations. In five cases, the anion was paired with a proton, *i.e.* the crystal structure was that of the free acid. In those cases, the agreement between theory and experiment was better when the *ab initio* model system was the free acid rather than the anion, Table 3. The overall RMSD in Table 3 was 10°, and reduced to 8° when only matching models were

considered. Even more, the RMSD among anionic crystal structures - excluding free acids - was as low as  $5^\circ$ . For comparison, an RMSD of  $5^\circ$  between experimental and theoretical structure corresponds to a distance of  $7^\circ$  in the 2D PES. The agreement between theory and experiment is excellent, given that the *ab initio* structures were obtained in vacuum, whereas the crystal structures are often thought to be dominated by packing effects. Here we were able to demonstrate the impressive predictive power of such simple calculations for the solid state, and it appears reasonable to assume equal or better agreement for the liquid state in which the thermal sampling of the PES is much less restricted by packing and geometry.

Table 2: Single crystal XRD data summary.

Sample ID	H[NMs <sub>2</sub> ]	[N <sub>1111</sub> ][NMs <sub>2</sub> ]	Li[NTfMs]	H[NTfMs]	[C <sub>4</sub> C <sub>1</sub> im][NMs <sub>2</sub> ]
Formula	C <sub>2</sub> H <sub>7</sub> NO <sub>4</sub> S <sub>2</sub>	C <sub>6</sub> H <sub>19</sub> N <sub>2</sub> O <sub>4</sub> S <sub>2</sub>	C <sub>2</sub> H <sub>3</sub> F <sub>3</sub> LiNO <sub>4</sub> S <sub>2</sub>	C <sub>2</sub> H <sub>4</sub> F <sub>3</sub> NO <sub>4</sub> S <sub>2</sub>	C <sub>10</sub> H <sub>21</sub> N <sub>3</sub> O <sub>4</sub> S <sub>2</sub>
CCDC Numbers	2175902	2175903	2175904	2175905	2175906
M / g mol <sup>-1</sup>	173.21	247.35	233.11	227.18	311.42
Crystal system	Monoclinic	Orthorhombic	Orthorhombic	Orthorhombic	Monoclinic
Space group (No.)	P2 <sub>1</sub> /c (14)	P2 <sub>1</sub> 2 <sub>1</sub> 2 <sub>1</sub> (19)	P2 <sub>1</sub> 2 <sub>1</sub> 2 <sub>1</sub> (19)	Pca2 <sub>1</sub>	P2 <sub>1</sub> /c (14)
a / Å	7.7622(5)	9.8237(3)	7.57011(19)	18.0557(4)	16.9703(9)
b / Å	9.9621(5)	10.7481(3)	8.4414(2)	9.23614(19)	8.3498(4)
c / Å	9.2314(5)	11.3025(4)	12.8321(4)	9.6547(2)	10.6415(6)
α / °	90	90	90	90	90
β / °	111.102(7)	90	90	90	98.565(5)
γ / °	90	90	90	90	90
U / Å <sup>3</sup>	665.97(7)	1193.39(6)	820.00(4)	1610.06	1491.07(14)
Z	4	4	4	8	4
m(Mo-Kα) / mm <sup>-1</sup>	0.745	0.44	0.681	0.692	0.37
F(000)	360	532	464	912	664
Total reflections	2280	15824	10536	19993	3142
Unique reflections	1324	2712	1842	3585	3142
R <sub>int</sub>	0.0227	0.0548	0.0213	0.0291	
GooF on F <sub>2</sub>	1.092	1.066	1.053	1.105	1.121
R <sub>1b</sub> [I <sub>o</sub> > 2s(I <sub>o</sub> )]	0.038	0.0403	0.0249	0.0269	0.055
R <sub>1</sub> (all data)	0.0513	0.0526	0.0263	0.0314	0.0656
wR <sub>2b</sub> [I <sub>o</sub> > 2s(I <sub>o</sub> )]	0.0826	0.093	0.0622	0.0593	0.1235
wR <sub>2</sub> (all data)	0.0905	0.1022	0.0632	0.0618	0.1287

Table 3: Experimental (X-ray crystallography) *vs* theoretical (*ab initio* simulation) dihedral angles for anions.

Experimental crystal structure			<i>ab initio</i> predicted structure			RMSD / °
Compound	$\phi_1 / ^\circ$	$\phi_2 / ^\circ$	Model	$\phi_1 / ^\circ$	$\phi_2 / ^\circ$	
H[NTfAc]	84	169	[NTfAc] <sup>-</sup>	58	169	18.5
H[NTfAc]	84	169	H[NTfAc]	78	171	4.6
K[NTfAc]	180	180	[NTfAc] <sup>-</sup>	180	180	0.0
H[NTFAMs]	181	61	[NTFAMs] <sup>-</sup>	179	50	7.7
H[NTFAMs]	181	61	H[NTFAMs]	171	61	7.2
H[NMsAc]	58	179	[NMsAc] <sup>-</sup>	51	174	5.7
H[NMsAc]	58	179	H[NMsAc]	64	164	11.5
[N1111][CHTf <sub>2</sub> ]	95	89	[CHTf <sub>2</sub> ] <sup>-</sup>	87	87	5.6
[N1111][CHTf <sub>2</sub> ]	94	88	[CHTf <sub>2</sub> ] <sup>-</sup>	87	87	4.7
[N1111][CHTf <sub>2</sub> ]	92	89	[CHTf <sub>2</sub> ] <sup>-</sup>	87	87	3.6
Li[NTfMs]	92	75	[NTfMs] <sup>-</sup>	88	65	7.7
H[NMs <sub>2</sub> ]	79	93	[NMs <sub>2</sub> ] <sup>-</sup>	72	72	15.4
H[NMs <sub>2</sub> ]	79	93	H[NMs <sub>2</sub> ]	68	78	12.8
[N1111][NMs <sub>2</sub> ]	76	75	[NMs <sub>2</sub> ] <sup>-</sup>	72	72	3.2
[C <sub>4</sub> C <sub>1</sub> im][NMs <sub>2</sub> ]	75	74	[NMs <sub>2</sub> ] <sup>-</sup>	72	72	2.9
H[NTfMs]	266	277	NTfMs	272	295	13.3
H[NTfMs]	265	282	NTfMs	272	295	10.4
H[NTfMs]	266	277	HNTfMs	282	286	12.7
H[NTfMs]	265	282	HNTfMs	282	286	11.9

The coordination environment of the cations in the crystal structure of  $[\text{C}_4\text{C}_1\text{im}][\text{NMs}_2]$  is shown in Figure 4. The anions show a number of close contacts to the (relatively) acidic hydrogen atoms near the imidazolium core. However, all of these hydrogen bonds are weak, see the geometric criteria in Table 4.<sup>14,15</sup> This is despite the  $[\text{NMs}_2]^-$  anion being reported to have much stronger hydrogen bonding than other imide anions, in particular  $[\text{NTf}_2]^-$ .<sup>5</sup>

Table 4: Hydrogen bond geometries obtained from the crystal structure of  $[\text{C}_4\text{C}_1\text{im}][\text{NMs}_2]$ . See also Figure 4; the order of the bonds follows the figure from top to bottom (first priority) and from left to right (second priority).

Type	Distance / Å			Angle
	H...A	C-H	C...A	C-H...A
A=O	2.54	0.97	3.44	154°
A=O	2.61	0.93	3.38	141°
A=N	2.42	0.93	3.32	161°
A=N	3.10	0.96	3.92	144°
A=O	2.58	0.96	3.52	165°
A=O	2.52	0.93	3.36	151°
A=N	2.94	0.93	3.40	111°
A=N	2.87	0.93	3.36	114°
A=O	2.91	0.93	3.79	159°

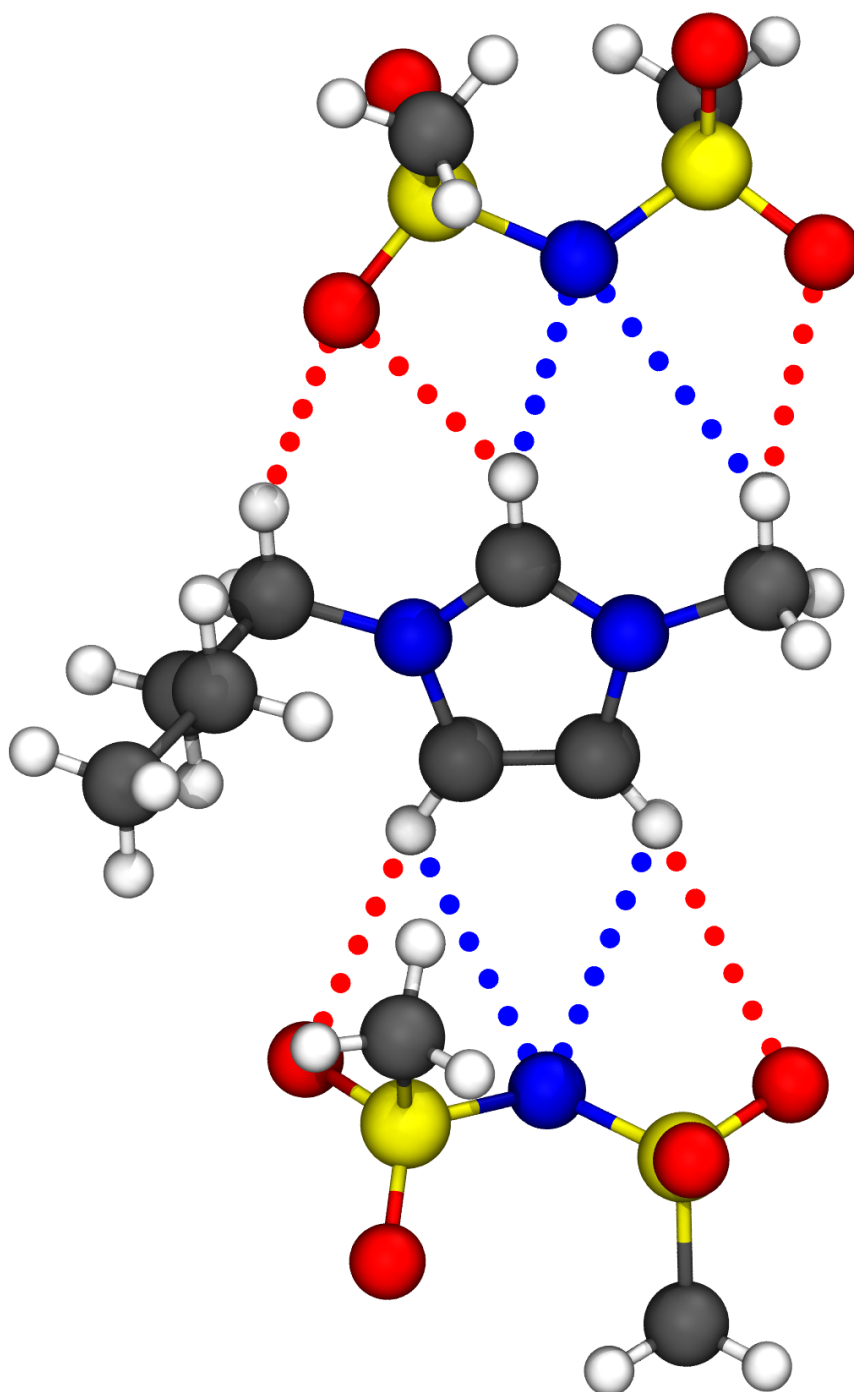


Figure 4: Configuration of  $[\text{NMs}_2]^-$  around  $[\text{C}_4\text{C}_1\text{im}]^+$  in the crystal structure of  $[\text{C}_4\text{C}_1\text{im}][\text{NMs}_2]$ . The imidazolium ring is in the paper plane. The anions (also in the paper plane) engage in a number of weak hydrogen bonds. Red dots highlight  $\text{O}\cdots\text{H}$  contacts, blue dots highlight  $\text{N}\cdots\text{H}$  contacts.

## 4 Physical Chemistry

### 4.1 Comparison with Literature Data

Table 5 gives an overview of the physicochemical properties of  $[\text{C}_4\text{C}_1\text{im}][\text{NTf}_2]$  in this work. This ionic liquid is amongst the most thoroughly investigated, Table 5 shows that our methods for synthesis and physicochemical measurements are reliable or at least consistent with the literature.

Table 5: Physicochemical properties of the  $[\text{C}_4\text{C}_1\text{im}][\text{NTf}_2]$  ionic liquid, comparison with literature data. All temperature dependent properties are given at 25°C.

Property	This work	Literature	Reference
Glass transition $T_g$	-88°C	-89°C	[16]
Cold crystallisation $T_{cc}$	-53°C	-53°C	[16]
Melting point $T_m$	-2°C	-4°C	[16]
Density $\rho$ / g cm <sup>-3</sup>	1.433(1)	1.436	[17]
$D_{self}^+$ / cm <sup>2</sup> s <sup>-1</sup>	$2.9(1) \times 10^{-7}$	$2.8 \times 10^{-7}$	[17]
$D_{self}^-$ / cm <sup>2</sup> s <sup>-1</sup>	$2.2(1) \times 10^{-7}$	$2.1 \times 10^{-7}$	[17]
Viscosity $\eta$ / mPa s	51(1)	51-52	[18, 19]
Conductivity $\kappa$ / mS cm <sup>-1</sup>	3.94(4)	3.94-4.04	[20]

### 4.2 Thermal Transitions

Thermal transitions measured *via* DSC are given in Table 6.  $[\text{C}_4\text{C}_1\text{im}][\text{NMs}_2]$  forms crystals, however nucleation is rarely observed. The melting point of  $[\text{C}_4\text{C}_1\text{im}][\text{NMs}_2]$  in the first heating cycle was found to be  $T_m = 49^\circ\text{C}$ . Only a glass transition is observed under the usual DSC conditions if a liquid sample is used (or after melting in the DSC). For the crystal structure of  $[\text{C}_4\text{C}_1\text{im}][\text{NMs}_2]$  Table 2.

Table 6: Thermal transitions of the ionic liquids in this work.

System	$T_g / ^\circ\text{C}$	$T_{cc} / ^\circ\text{C}$	$T_m / ^\circ\text{C}$	Type
$[\text{C}_4\text{C}_1\text{im}][\text{NTf}_2]$	-88	-53	-2	3
$[\text{C}_4\text{C}_1\text{im}][\text{CHTf}_2]$	-70	-16	18	3
$[\text{C}_4\text{C}_1\text{im}][\text{NTfAc}]$	-77	—	—	1
$[\text{C}_4\text{C}_1\text{im}][\text{NMsTFA}]$	-66	-16	-8	3
$[\text{C}_4\text{C}_1\text{im}][\text{NMs}_2]^a$	-52	—	—	1
$[\text{C}_4\text{C}_1\text{im}][\text{NTfMs}]$	-66	-17	-8	3
$[\text{C}_4\text{C}_1\text{im}][\text{NFs}_2]$	-100	-51	-37	3
$[\text{C}_4\text{C}_1\text{im}][6\text{cPFSI}]^b$	—	—	29	2
$[\text{C}_4\text{C}_1\text{im}][\text{NPf}_2]$	-85	—	—	1
$[\text{C}_4\text{C}_1\text{im}][\text{B}(\text{CN})_4]$	-76	—	—	1

<sup>a</sup> crystals of  $[\text{C}_4\text{C}_1\text{im}][\text{NMs}_2]$  show  $T_m = 49^\circ\text{C}$ .

<sup>b</sup>  $[\text{C}_4\text{C}_1\text{im}][6\text{cPFSI}]$  crystallised upon cooling,  $T_c = 1^\circ\text{C}$ .

### 4.3 Density

Experimental values for the density  $\rho$  are given in Table 7. The experimental data was fitted with linear equation, Equation 1, the fit parameters are given in Table 8.

$$\frac{\rho}{\text{g cm}^{-3}} = a + b \cdot \frac{T}{K} \quad (1)$$

Table 7: Experimental densities in  $\text{g cm}^{-3}$ .

Temperature / $^{\circ}\text{C}$	25	35	45	55	65	75	85	95
$[\text{C}_4\text{C}_1\text{im}][\text{NTf}_2]$	1.433	1.424	1.415	1.405	1.395	1.386	1.377	1.368
$[\text{C}_4\text{C}_1\text{im}][\text{CHTf}_2]$	1.419	1.410	1.400	1.391	1.382	1.372	1.363	1.354
$[\text{C}_4\text{C}_1\text{im}][\text{NTfAc}]$	1.271	1.263	1.255	1.247	1.239	1.231	1.223	1.216
$[\text{C}_4\text{C}_1\text{im}][\text{NMsTFA}]$	1.280	1.272	1.264	1.256	1.248	1.241	1.233	1.225
$[\text{C}_4\text{C}_1\text{im}][\text{NMs}_2]$	1.252	1.245	1.238	1.231	1.224	1.218	1.211	1.204
$[\text{C}_4\text{C}_1\text{im}][\text{NTfMs}]$	1.354	1.346	1.339	1.330	1.322	1.314	1.306	1.298
$[\text{C}_4\text{C}_1\text{im}][\text{NFs}_2]$	1.355	1.346	1.337	1.329	1.321	1.312	1.304	1.296
$[\text{C}_4\text{C}_1\text{im}][6\text{cPFSI}]$	1.484	1.476	1.467	1.457	1.448	1.439	1.430	1.421
$[\text{C}_4\text{C}_1\text{im}][\text{NPF}_2]$	1.511	1.500	1.490	1.479	1.469	1.459	1.449	1.439
$[\text{C}_4\text{C}_1\text{im}][\text{B}(\text{CN})_4]$	1.008	1.000	0.993	0.985	0.978	0.971	0.964	0.957

Table 8: Parameters of linear fit of experimental densities.

	a	$10^3 \cdot \Delta a$	$10^4 \cdot b$	$10^6 \cdot \Delta b$	Adj. $R^2$
$[\text{C}_4\text{C}_1\text{im}][\text{NTf}_2]$	1.712	1.560	-9.354	4.682	0.99982
$[\text{C}_4\text{C}_1\text{im}][\text{CHTf}_2]$	1.696	1.620	-9.308	4.850	0.99981
$[\text{C}_4\text{C}_1\text{im}][\text{NTfAc}]$	1.505	1.120	-7.862	3.352	0.99987
$[\text{C}_4\text{C}_1\text{im}][\text{NMsTFA}]$	1.514	0.801	-7.857	2.399	0.99993
$[\text{C}_4\text{C}_1\text{im}][\text{NMs}_2]$	1.454	0.763	-6.791	2.285	0.99992
$[\text{C}_4\text{C}_1\text{im}][\text{NTfMs}]$	1.594	1.420	-8.041	4.248	0.99980
$[\text{C}_4\text{C}_1\text{im}][\text{NFs}_2]$	1.602	1.320	-8.322	3.958	0.99984
$[\text{C}_4\text{C}_1\text{im}][6\text{cPFSI}]$	1.757	3.220	-9.150	9.638	0.99922
$[\text{C}_4\text{C}_1\text{im}][\text{NPF}_2]$	1.817	0.717	-10.300	2.147	0.99997
$[\text{C}_4\text{C}_1\text{im}][\text{B}(\text{CN})_4]$	1.222	1.190	-7.185	3.554	0.99983

## 4.4 Viscosity

Experimental values for the viscosities  $\eta$  are given in Table 10. The experimental data was fitted with a Vogel-Fulcher-Tammann equation, Equation 2, the fit parameters are given in Table 9.

$$\eta = \eta_0 \exp\left(\frac{B}{T - T_0}\right) \quad (2)$$

Table 9: VFT Fit parameters of experimental viscosities.

	$\eta_0$ / mPa s	$\Delta\eta_0$ / %	B / K	$\Delta B$ / %	$T_0$ / K	$\Delta T_0$ / %	$R^2$
[C <sub>4</sub> C <sub>1</sub> im][NTf <sub>2</sub> ]	0.19591	2.80	704.92	1.18	171.28	0.51	0.99999
[C <sub>4</sub> C <sub>1</sub> im][CHTf <sub>2</sub> ]	0.15131	1.99	741.75	0.66	190.97	0.21	1.00000
[C <sub>4</sub> C <sub>1</sub> im][NTfAc]	0.12062	3.19	813.35	1.03	183.68	0.37	1.00000
[C <sub>4</sub> C <sub>1</sub> im][NMsTFA]	0.13376	3.05	787.57	0.91	195.55	0.27	1.00000
[C <sub>4</sub> C <sub>1</sub> im][NMs <sub>2</sub> ]	0.08158	9.27	969.18	2.13	197.64	0.60	0.99999
[C <sub>4</sub> C <sub>1</sub> im][NTfMs]	0.14359	2.37	815.18	0.77	183.42	0.27	1.00000
[C <sub>4</sub> C <sub>1</sub> im][NFs <sub>2</sub> ]	0.18639	0.79	723.80	0.36	158.36	0.18	1.00000
[C <sub>4</sub> C <sub>1</sub> im][6cPFSI]	0.14407	1.62	872.42	0.52	175.05	0.21	1.00000
[C <sub>4</sub> C <sub>1</sub> im][NPf <sub>2</sub> ]	0.10394	3.81	910.23	1.24	168.52	0.54	0.99999
[C <sub>4</sub> C <sub>1</sub> im][B(CN) <sub>4</sub> ]	0.19981	1.38	547.21	0.65	189.89	0.22	1.00000

Table 10: Experimental viscosities in mPa s.

Temperature / °C	25	30	35	40	45	50	55	60	65	70	75	80	85	90	95	100	105
[C <sub>4</sub> C <sub>1</sub> im][NTf <sub>2</sub> ]	50.7	41.1	33.7	28.2	23.8	20.3	17.6	15.3	13.4	11.9	10.5	9.45	8.52	7.71	7.00	6.41	5.88
[C <sub>4</sub> C <sub>1</sub> im][CHTf <sub>2</sub> ]	153	113	84.9	65.5	51.7	41.4	33.7	27.8	23.3	19.7	16.9	14.7	12.8	11.3	10.0	8.95	8.05
[C <sub>4</sub> C <sub>1</sub> im][NTfAc]	147	109	83.1	64.6	51.0	41.1	33.5	27.8	23.3	19.8	16.9	14.7	12.8	11.3	10.0	8.90	7.98
[C <sub>4</sub> C <sub>1</sub> im][NMsTFA]	288	202	146	108	82.3	63.9	50.7	40.8	33.4	27.7	23.3	19.8	17.0	14.8	13.0	11.4	10.2
[C <sub>4</sub> C <sub>1</sub> im][NMs <sub>2</sub> ]	1256	799	526	358	252	183	136	104	80.6	63.9	51.5	42.3	35.0	29.3	24.9	21.4	18.5
[C <sub>4</sub> C <sub>1</sub> im][NTfMs]	175	130	98.8	77.0	60.9	49.1	40.1	33.1	27.9	23.6	20.2	17.5	15.3	13.4	11.9	10.6	9.5
[C <sub>4</sub> C <sub>1</sub> im][NFs <sub>2</sub> ]	33.0	27.6	23.4	20.0	17.3	15.1	13.2	11.7	10.5	9.37	8.45	7.65	6.97	6.39	5.87	5.42	5.02
[C <sub>4</sub> C <sub>1</sub> im][6cPFSI]	172	131	101	79.8	64.0	52.1	43.0	35.9	30.3	25.8	22.2	19.3	16.9	14.9	13.2	11.8	10.6
[C <sub>4</sub> C <sub>1</sub> im][NPf <sub>2</sub> ]	116	89.9	70.5	56.3	45.5	37.4	31.0	26.1	22.2	19.1	16.5	14.4	12.7	11.2	9.97	8.93	8.05
[C <sub>4</sub> C <sub>1</sub> im][B(CN) <sub>4</sub> ]	31.3	25.0	20.4	16.9	14.2	12.1	10.5	9.12	8.02	7.11	6.36	5.71	5.16	4.70	4.30	3.94	3.63

## 4.5 Conductivity

Experimental values for the molar conductivities  $\Lambda$  are given in Table 12 and Table 13. The experimental data was fitted with a Vogel-Fulcher-Tammann equation, Equation 3, the fit parameters are given in Table 11.

$$\Lambda = \Lambda_0 \exp\left(\frac{B}{T - T_0}\right) \quad (3)$$

Table 11: VFT fit parameters of experimental conductivities.

	$\Lambda_0 / \text{mS cm}^{-1}$	$\Delta\Lambda_0 / \%$	$B / \text{K}$	$\Delta B / \%$	$T_0 / \text{K}$	$\Delta T_0 / \%$	$R^2$
$[\text{C}_4\text{C}_1\text{im}][\text{NTf}_2]$	425.6	2.51	-559.0	1.45	178.88	0.65	0.99999
$[\text{C}_4\text{C}_1\text{im}][\text{CHTf}_2]$	435.1	1.68	-565.2	0.85	199.79	0.30	1.00000
$[\text{C}_4\text{C}_1\text{im}][\text{NTfAc}]$	594.2	1.96	-640.3	0.93	191.91	0.36	1.00000
$[\text{C}_4\text{C}_1\text{im}][\text{NMsTFA}]$	508.6	5.18	-591.1	2.42	207.75	0.79	0.99997
$[\text{C}_4\text{C}_1\text{im}][\text{NMs}_2]$	607.4	7.55	-658.0	3.07	215.30	0.95	0.99997
$[\text{C}_4\text{C}_1\text{im}][\text{NTfMs}]$	628.1	2.45	-682.4	1.13	187.49	0.47	0.99999
$[\text{C}_4\text{C}_1\text{im}][\text{NFs}_2]$	526.7	3.60	-530.1	2.28	171.63	1.10	0.99998
$[\text{C}_4\text{C}_1\text{im}][6\text{cPF6SI}]$	592.5	1.74	-737.7	0.78	179.00	0.35	1.00000
$[\text{C}_4\text{C}_1\text{im}][\text{NPF}_2]$	422.2	3.97	-656.1	1.93	183.72	0.83	0.99998
$[\text{C}_4\text{C}_1\text{im}][\text{B}(\text{CN})_4]$	545.5	5.67	-467.4	3.63	190.53	1.40	0.99993

Table 12: Experimental conductivities in  $\text{mS cm}^{-1}$ .

Temperature / °C	25	30	35	40	45	50	55	60
$[\text{C}_4\text{C}_{1\text{im}}][\text{NTf}_2]$	3.936	4.740	5.623	6.608	7.684	8.834	10.061	11.366
$[\text{C}_4\text{C}_{1\text{im}}][\text{CHTf}_2]$	1.395	1.841	2.368	2.968	3.669	4.458	5.316	6.268
$[\text{C}_4\text{C}_{1\text{im}}][\text{NTfAc}]$	1.444	1.883	2.407	3.015	3.730	4.526	5.404	6.378
$[\text{C}_4\text{C}_{1\text{im}}][\text{NMsTFA}]$	0.769	1.063	1.423	1.865	2.394	3.003	3.711	4.548
$[\text{C}_4\text{C}_{1\text{im}}][\text{NMs}_2]$	0.236	0.355	0.518	0.736	1.012	1.361	1.776	2.262
$[\text{C}_4\text{C}_{1\text{im}}][\text{NTfMs}]$	1.316	1.717	2.191	2.751	3.397	4.122	4.918	5.794
$[\text{C}_4\text{C}_{1\text{im}}][\text{NFs}_2]$	8.003	9.342	10.823	12.429	14.134	15.933	17.799	19.774
$[\text{C}_4\text{C}_{1\text{im}}][6\text{cPFSI}]$	1.213	1.554	1.955	2.419	2.952	3.559	4.225	4.952
$[\text{C}_4\text{C}_{1\text{im}}][\text{NPf}_2]$	1.389	1.757	2.169	2.637	3.192	3.801	4.496	5.222
$[\text{C}_4\text{C}_{1\text{im}}][\text{B}(\text{CN})_4]$	7.092	8.612	10.273	12.103	14.062	16.086	18.287	20.490

Table 13: Experimental conductivities in  $\text{mS cm}^{-1}$  - continued.

Temperature / °C	65	70	75	80	85	90	95	100
$[\text{C}_4\text{C}_{1\text{im}}][\text{NTf}_2]$	12.750	14.143	15.666	17.240	18.825	20.470	22.155	23.989
$[\text{C}_4\text{C}_{1\text{im}}][\text{CHTf}_2]$	7.316	8.439	9.633	10.917	12.272	13.687	15.169	16.675
$[\text{C}_4\text{C}_{1\text{im}}][\text{NTfAc}]$	7.448	8.609	9.852	11.211	12.643	14.141	15.710	17.347
$[\text{C}_4\text{C}_{1\text{im}}][\text{NMsTFA}]$	5.467	6.462	7.573	8.770	9.991	11.329	12.760	14.253
$[\text{C}_4\text{C}_{1\text{im}}][\text{NMs}_2]$	2.840	3.525	4.302	5.145	6.085	7.092	8.232	9.368
$[\text{C}_4\text{C}_{1\text{im}}][\text{NTfMs}]$	6.750	7.842	8.976	10.203	11.529	12.920	14.381	15.901
$[\text{C}_4\text{C}_{1\text{im}}][\text{NFs}_2]$	21.849	24.000	26.021	28.452	30.762	33.005	35.458	37.966
$[\text{C}_4\text{C}_{1\text{im}}][6\text{cPFSI}]$	5.746	6.621	7.556	8.564	9.645	10.789	12.004	13.256
$[\text{C}_4\text{C}_{1\text{im}}][\text{NPF}_2]$	6.012	6.903	7.829	8.800	9.825	10.911	12.032	13.211
$[\text{C}_4\text{C}_{1\text{im}}][\text{B}(\text{CN})_4]$	22.816	25.502	28.108	31.065	33.598	36.438	39.284	42.099

## 4.6 Diffusion Coefficients

Experimental values for the self-diffusion coefficients of cation  $D^+$  and anion  $D^-$  are given in Table 14.

Table 14: Experimental diffusion coefficients in  $\text{cm}^2\text{s}^{-1}$ .

	Measured at T = 25°C			Measured at T = 35°C		
	$D^+(\text{}^1\text{H})$	$D^-(\text{}^{19}\text{F})$	$D^-(\text{}^1\text{H})$	$D^+(\text{}^1\text{H})$	$D^-(\text{}^{19}\text{F})$	$D^-(\text{}^1\text{H})$
$[\text{C}_4\text{C}_1\text{im}][\text{NTf}_2]$	$2.85 \cdot 10^{-7}$	$2.16 \cdot 10^{-7}$	—	$4.44 \cdot 10^{-7}$	$3.38 \cdot 10^{-7}$	—
$[\text{C}_4\text{C}_1\text{im}][\text{CHTf}_2]$	$9.79 \cdot 10^{-8}$	$7.92 \cdot 10^{-8}$	—	$1.82 \cdot 10^{-7}$	$1.50 \cdot 10^{-7}$	—
$[\text{C}_4\text{C}_1\text{im}][\text{NTfAc}]$	$1.01 \cdot 10^{-7}$	$7.66 \cdot 10^{-8}$	$7.72 \cdot 10^{-8}$	$1.89 \cdot 10^{-7}$	$1.44 \cdot 10^{-7}$	$1.47 \cdot 10^{-7}$
$[\text{C}_4\text{C}_1\text{im}][\text{NMsTFA}]$	$5.03 \cdot 10^{-8}$	$4.12 \cdot 10^{-8}$	$4.21 \cdot 10^{-8}$	$1.04 \cdot 10^{-7}$	$8.62 \cdot 10^{-8}$	$8.67 \cdot 10^{-8}$
$[\text{C}_4\text{C}_1\text{im}][\text{NMs}_2]^{\text{a}}$	—	—	—	$3.33 \cdot 10^{-8}$	—	$2.82 \cdot 10^{-8}$
$[\text{C}_4\text{C}_1\text{im}][\text{NMs}_2]^{\text{b}}$	—	—	—	$3.36 \cdot 10^{-8}$	—	$2.85 \cdot 10^{-8}$
$[\text{C}_4\text{C}_1\text{im}][\text{NTfMs}]$	$8.57 \cdot 10^{-8}$	$6.36 \cdot 10^{-8}$	$6.52 \cdot 10^{-8}$	$1.52 \cdot 10^{-7}$	$1.16 \cdot 10^{-7}$	$1.17 \cdot 10^{-7}$
$[\text{C}_4\text{C}_1\text{im}][\text{NFs}_2]$	$4.17 \cdot 10^{-7}$	$4.07 \cdot 10^{-7}$	—	$6.12 \cdot 10^{-7}$	$6.00 \cdot 10^{-7}$	—
$[\text{C}_4\text{C}_1\text{im}][6\text{cPFSI}]$	$9.37 \cdot 10^{-8}$	$6.00 \cdot 10^{-8}$	—	—	—	—
$[\text{C}_4\text{C}_1\text{im}][\text{NPf}_2]$	$1.29 \cdot 10^{-7}$	$8.83 \cdot 10^{-8}$	—	$2.21 \cdot 10^{-7}$	$1.53 \cdot 10^{-7}$	—
$[\text{C}_4\text{C}_1\text{im}][\text{B}(\text{CN})_4]$	$4.23 \cdot 10^{-7}$	—	—	$6.74 \cdot 10^{-7}$	—	—

<sup>a</sup> Parameters optimised for anion diffusion measurement.

<sup>b</sup> Parameters optimised for cation diffusion measurement.

## 4.7 DMTA Measurements

Dynamic mechanical thermal analysis (DMTA) was carried out using a PerkinElmer DMA 8000 instrument, by means of a method already used in previous works<sup>21,22</sup>: the liquid samples were laid out at room temperature into a stainless steel Material Pocket, supplied by PerkinElmer (30.0 mm by 14.0 mm by 0.5 mm), which is then folded in half and crimped closed. Flexural vibration measurements were performed in the three-point bending configuration. The storage modulus,  $E$ , and the elastic energy dissipation,  $\tan \delta = E''/E'$ , were measured at variable frequencies (1 Hz and 10 Hz) and scanning temperature at 4 K min<sup>-1</sup>. The stress applied by this method is not a pure shear stress, but, due to the spatial isotropy of liquids, the mechanical modulus presently measured is a combination of both the shear and the bulk modulus.<sup>23,24</sup>

The discussion in the main manuscript is based on a two site model. In other words, it is assumed that the mechanism of relaxation requires a transition between two nonequivalent configurations with an asymmetric potential profile. When species can move between two configurations with a relaxation rate  $\tau^{-1}$  by means of thermal activation in a standard anelastic solid,<sup>25</sup> the elastic energy dissipation presents a maximum when the Debye relaxation condition,  $\omega\tau = 1$ , is satisfied. For a single relaxation time  $\tau$ ,  $\tan \delta$  is given by Equation 4.

$$\tan \delta = \frac{\Delta(T)}{(\omega\tau)^\alpha + (\omega\tau)^{-\alpha}} \quad (4)$$

Here,  $\omega$  is the angular vibration frequency. The relaxation intensity  $\Delta(T)$  is proportional to the concentration of the relaxing species, to the elastic modulus and to the change in the local distortion,  $\alpha$  is the Fuoss–Kirkwood width parameter and is equal to 1 for a single time Debye relaxation;  $\alpha < 1$  produces broadened peaks with respect to Debye ones.<sup>25</sup>

The rate of this transition is characterised by a temperature dependent relaxation time  $\tau$ , Equation 5. Here, the Vogel-Fulcher-Tammann (VFT) equation is used to describe the temperature dependence;  $\tau_0$ ,  $B$  and  $T_0$  are parameters.<sup>26–28</sup> This approach is common for ionic liquids, which in most cases show significant deviation from Arrhenius behaviour in their dynamic properties around or below room temperature.<sup>29–34</sup> The parameter  $B$  can be interpreted as apparent activation energy  $W$ , in analogy with the Arrhenius equation (which is recovered for  $T_0 = 0$  K).

$$\tau = \tau_0 \exp\left(\frac{B}{T - T_0}\right) = \tau_0 \exp\left(\frac{W}{R(T - T_0)}\right) \quad (5)$$

The relaxation time  $\tau$  changes dramatically with temperature. Thus, information about the relaxation behaviour can be obtained by changing the temperature at different frequencies

of the oscillating deformation  $f$ . If the relaxation occurs between two equivalent sites, the relaxation intensity in Equation 4 decreases with increasing  $T$ , leading to a higher intensity for the peaks measured at lower frequencies.

For the two (non equivalent) site model, the relaxation intensity is proportional to the product of the respective populations in the two configurations and the thermally activated peak in the loss tangent can be fitted with Equation 6.<sup>21,22,35,36</sup>

$$\tan \delta = \frac{c}{T} \operatorname{sech}^2 \left( \frac{\Delta E}{2RT} \right) \frac{(\omega\tau)^\alpha}{1 + (\omega^2\tau^2)^\alpha} \quad (6)$$

Here, the blue part is the relaxation intensity  $\Delta(T)$  in Equation 4, and  $c$  is a collective fit parameter.  $\Delta E$  is the energy difference between the two non equivalent sites. The fit parameters are shown in Table 15.

Table 15: DMTA fit parameters.

Ionic liquid	T0/K	$\alpha$	$\Delta E / \text{kJ mol}^{-1}$	$\tau_0 / \text{s}$	$W / \text{kJ mol}^{-1}$
[C <sub>4</sub> C <sub>1</sub> Im][NTf <sub>2</sub> ]	85(4)	0.7(1)	2.6(3)	1.6(2)·10 <sup>-13</sup>	31(2)
[C <sub>4</sub> C <sub>1</sub> Im][NTfAc]	64(2)	0.7(1)	1.64(22)	1.7(2)·10 <sup>-13</sup>	41(1)
[C <sub>4</sub> C <sub>1</sub> Im][NMsTFA]	70(3)	0.7(1)	11.6(39)	4.0(1)·10 <sup>-13</sup>	41(1)
	70(3)	1	4.1(5)	4.0(1)·10 <sup>-13</sup>	46(1)
[C <sub>4</sub> C <sub>1</sub> Im][NMs <sub>2</sub> ]	115(2)	1	15(2)	1.0(1)·10 <sup>-13</sup>	35(4)
[C <sub>4</sub> C <sub>1</sub> Im][NTfMs]	52(4)	0.85(5)	4.7(2)	2.3(5)·10 <sup>-13</sup>	43(1)
[C <sub>4</sub> C <sub>1</sub> Im][B(CN) <sub>4</sub> ]	190(4)	0.6(1)	0	2.4(9)·10 <sup>-6</sup>	2.3(1)

The  $\tan \delta$  experimental data and fit curves are shown in Figure 5. The  $\tan \delta$  experimental data and fit curves for [C<sub>4</sub>C<sub>1</sub>im][B(CN)<sub>4</sub>] are shown in Figure 6. The analysis was not possible for the DMTA spectra presented in Figure 7. For [C<sub>4</sub>C<sub>1</sub>im][NFs<sub>2</sub>], the low temperature side of the peaks measured at two different frequencies are superimposed. For the other two ionic liquids, [C<sub>4</sub>C<sub>1</sub>im][6cPFSI] and [C<sub>4</sub>C<sub>1</sub>im][CHTf<sub>2</sub>], a phase transition occurs which does not allow the detection of the thermally activated relaxation.

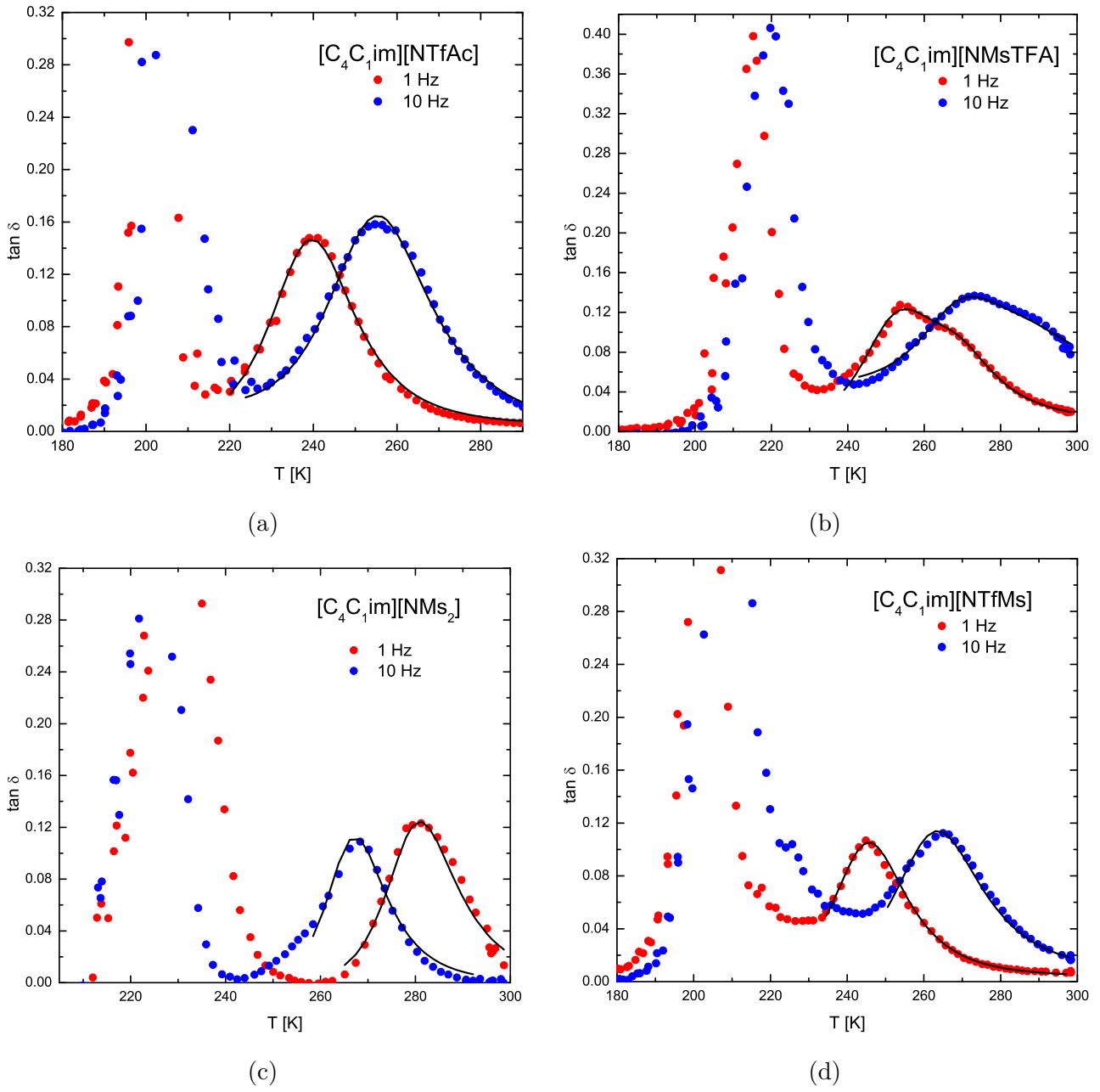


Figure 5:  $\tan \delta$  experimental data measured on cooling (scatter plot) and curve fits (line plot).

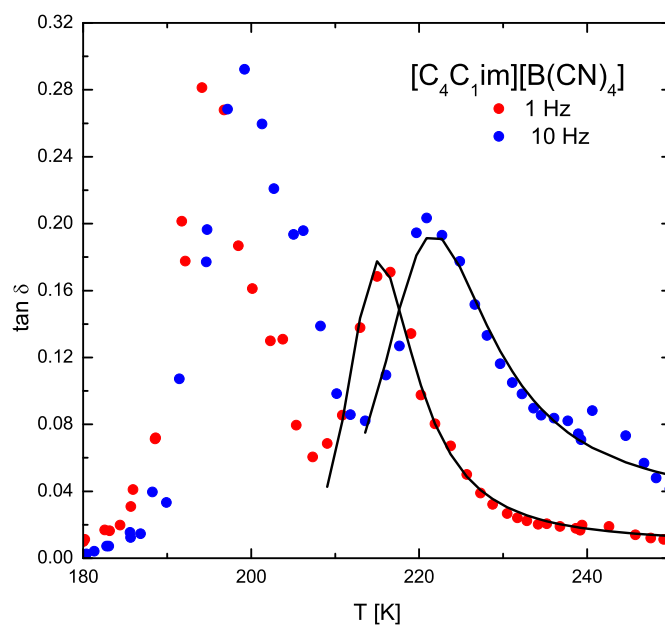
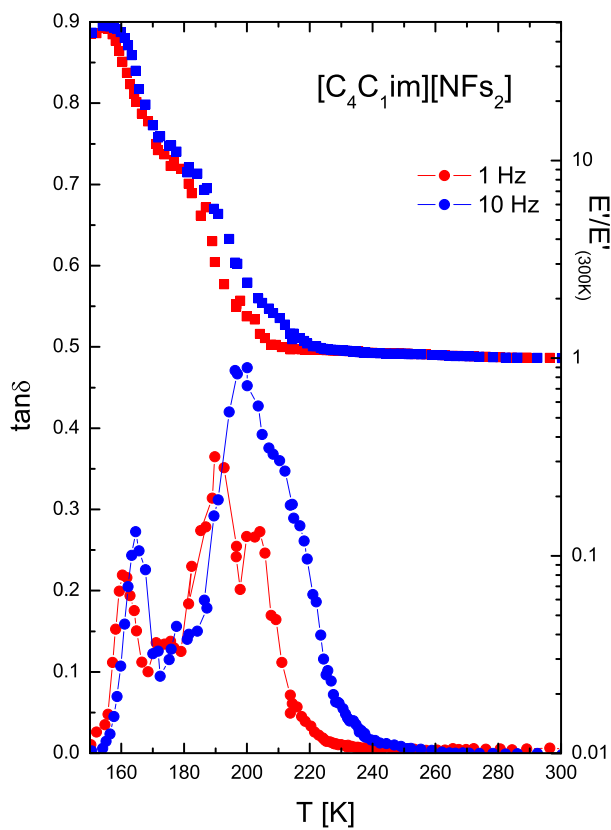
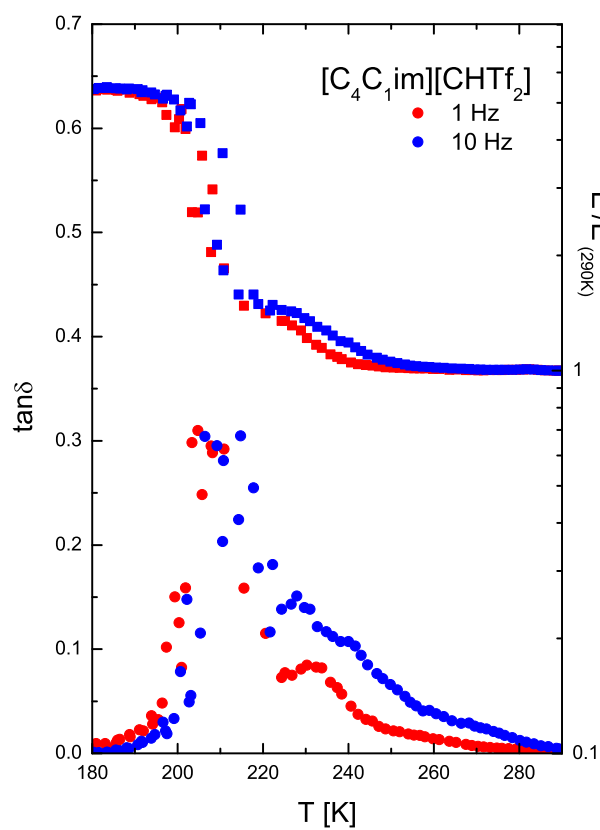


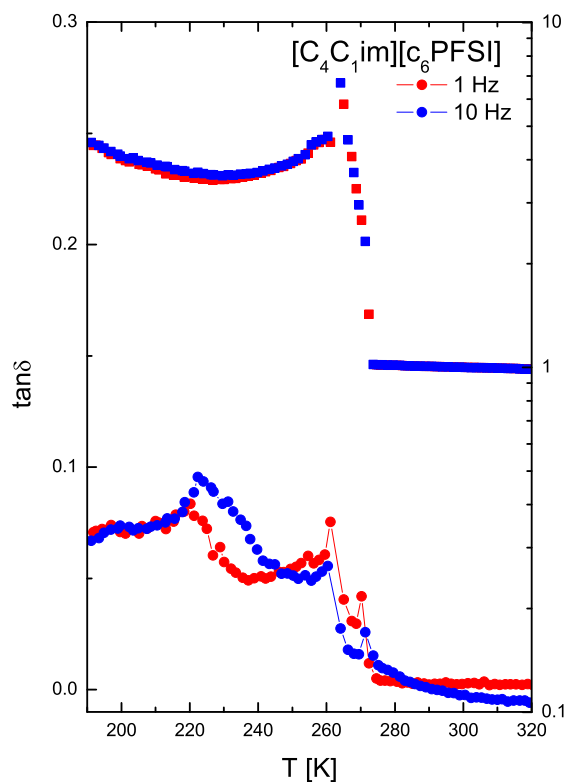
Figure 6:  $\tan \delta$  experimental data for  $[\text{C}_4\text{C}_1\text{im}][\text{B}(\text{CN})_4]$  measured on cooling (scatter plot) and curve fits (line plot).



(a)



(b)



(c)

Figure 7: Experimental DMTA spectra which could not be fitted. Squares are relative  $E'$ , circles are  $\tan \delta$ . Lines are a guide for the eye.

## 5 MD simulations

### 5.1 MD simulation details

Periodic boundary conditions were used throughout, with a cutoff of 12 Å for both Coulomb and 12/6 Lennard-Jones interactions. Beyond 12 Å, Coulomb interactions were calculated with a particle-particle particle-mesh solver with  $10^{-6}$  relative error in per-atom forces. A Van der Waals tail correction was also included.<sup>37</sup> Non-bonded interactions (Coulomb and Lennard-Jones) were scaled by factors 0.0, 0.0, 0.5 for pairs of atoms which are exactly 1, 2, 3 bonds apart. Lennard-Jones parameters between pairs of atoms of differing type were obtained by geometric mixing. Neighbour lists were created by binning with a skin distance of 2.0 Å. The equations of motion were integrated using the velocity-Verlet method with a timestep of 0.5 fs. Bond constraints (for C-H bonds) were enforced with the SHAKE algorithm with a maximum of 20 iterations and a tolerance of  $10^{-4}$ .<sup>38</sup> The centre of mass momentum over all contents of the simulation box was subtracted every 1000 timesteps.

Drude particles were added to non-hydrogen atoms to emulate polarisability.<sup>39,40</sup> The Drude particles have a mass of 0.4 Da and a charge of  $q_{Drude} = \sqrt{\alpha k_{Drude}}$ . Here,  $\alpha$  is the atomic polarisability.<sup>41</sup> Drude particles and cores are connected with a harmonic potential with 0.0 Å equilibrium distance and spring constant  $k_{Drude} = 1000 \text{ kcal mol}^{-1} = 4184 \text{ kJ mol}^{-1}$ .<sup>42</sup> Thole damping with  $\alpha = 2.6$  was used.<sup>39,43</sup>

The temperature-grouped Nosé-Hoover chain thermostat (barostat, including the Martyna-Tuckerman-Klein correction<sup>44</sup>) with chain length of three was used for temperature (pressure) control.<sup>45</sup> Atomic degrees of freedom and molecular centre of mass motion were kept at a given temperature with a damping parameter of 100 fs (1 ps for pressure), while the internal motions of Drude-core pairs was thermostatted at 1 K with a damping parameter of 25 fs.<sup>42,46</sup> Simulations of [C<sub>4</sub>C<sub>1</sub>im][NTf<sub>2</sub>] and [C<sub>4</sub>C<sub>1</sub>im][CHTf<sub>2</sub>] were run, both at 298 K and 333 K. The pressure in NPT ensembles was set to 1 bar. Heating/cooling was performed in linear ramps.

For the [C<sub>4</sub>C<sub>1</sub>im][NTf<sub>2</sub>] ionic liquid, additional simulations at 333 K were run with the [NTf<sub>2</sub>]<sup>-</sup> anion fixed in a certain conformation, using the PLUMED software package version 2.6.0.<sup>47-49</sup> For each of the 512 anions, the two C-S-N-S dihedrals were defined using the ‘TORSION’ collective variable. Harmonic restraints were placed on the dihedral angles using the ‘RESTRAINT’ keyword. The initial topology was that of the native CL&Pol/TG-NH after the

production run. Starting from this topology, the whole procedure with minimisation, annealing, isobaric-isothermal equilibration, isothermal equilibration, and finally production run was repeated with the respective constraints turned on.

Prior to the simulation, 512 ion pairs were randomly packed into a cubic box using PACKMOL,<sup>50</sup> the energy minimised (conjugate gradient minimiser, maximum 100 steps,  $10^{-4}$  stopping tolerance for energy,  $10^{-6}$  kcal mol<sup>-1</sup> Å<sup>-1</sup> stopping tolerance for force), and the atoms assigned random velocities corresponding to the thermostat target temperature.

The following annealing/equilibration/production procedure was used for all polarisable simulations. The system was kept at the target temperature for 50 ps, heated to 600 K over 50 ps, kept at 600 K for 100 ps, cooled to the target temperature over 50 ps. The annealing (250 ps) was performed in the NPT ensemble. Then, the system was kept at the target temperature for 25 ps in NVT, and for 150 ps in NPT. The box size in the NPT run was recorded every 10 steps and averaged over the 150 ps. This sequence - 25 ps in NVT and 150 ps in NPT - was repeated 10-20 times. After confirming the absence of drift in the local averages of the box size, the box was compressed to the overall (global) average box size over 25 ps, and equilibrated in NVT for 4 ns. Finally, a production run followed, recording the trajectory every 1 ps. After the production run, the simulation was continued for an additional 50 ps, recording the trajectory every 1 fs for the study of short time behaviour (*e.g.* for  $\alpha_2$  and time correlation functions).

The production runs for each of the polarisable simulations were 20 ns for [C<sub>4</sub>C<sub>1</sub>im][CHTf<sub>2</sub>] at 298 K and 333 K; 20 ns for [C<sub>4</sub>C<sub>1</sub>im][NTf<sub>2</sub>] at 298 K and 10 ns for [C<sub>4</sub>C<sub>1</sub>im][NTf<sub>2</sub>] at 333 K; 20 ns for the simulations of [C<sub>4</sub>C<sub>1</sub>im][NTf<sub>2</sub>] at 333 K where the anions were restrained to the *cis* conformers / *trans* conformers / a mixture of both.

## 5.2 Force Field

For the [C<sub>4</sub>C<sub>1</sub>im]<sup>+</sup> cation and the [NTf<sub>2</sub>]<sup>-</sup> anion, unchanged literature CL&Pol force field parameters were used.<sup>40,51-53</sup> The force field for the [CHTf<sub>2</sub>]<sup>-</sup> anion was created as follows. CHELPG charges<sup>54</sup> constrained to reproduce the dipole moment were calculated for both the *cis* and *trans* [CHTf<sub>2</sub>]<sup>-</sup> structures, fitting the MP2 ESP at the full MP2/cc-pVTZ//B3LYP-GD3BJ/6-311+G(d,p) level of theory. The atoms in the CF<sub>3</sub> group gave virtually identical charge values as for [NTf<sub>2</sub>]<sup>-</sup> in the CL&P implementation, hence the latter was kept. For all other atoms, the fitted CHELPG charges were used rounded to two digits, and +0.01 e were added to the

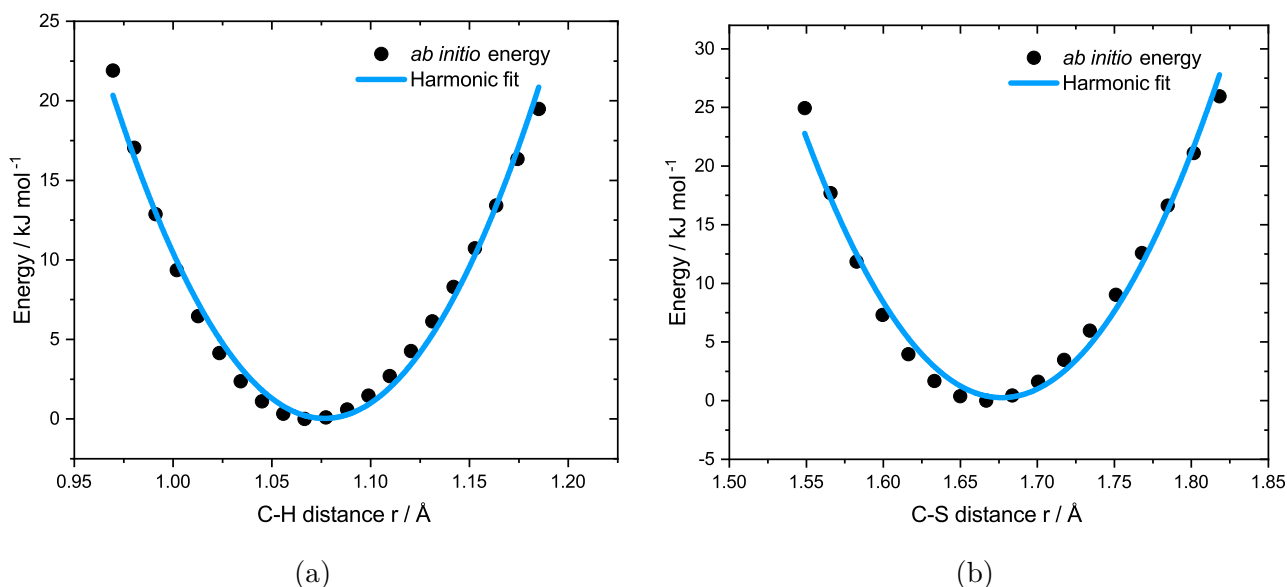
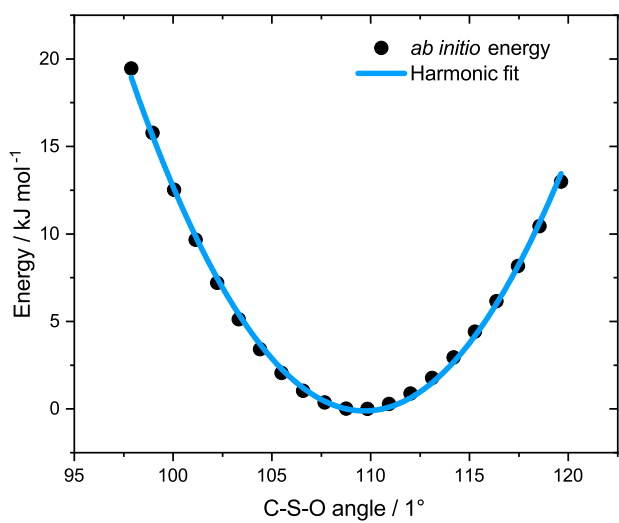


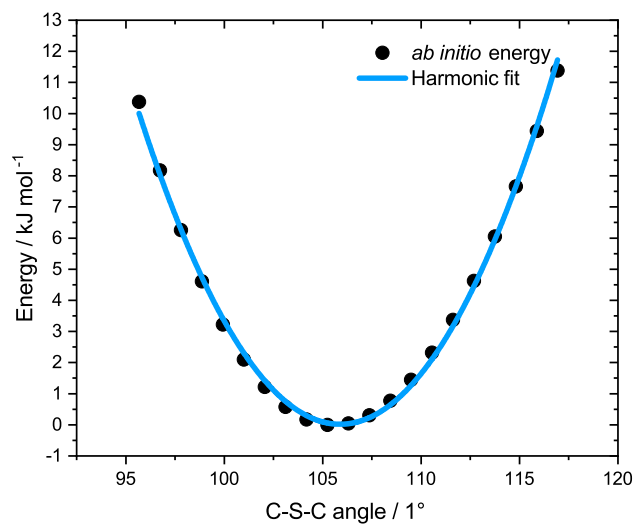
Figure 8: Fits for bond stretching constants in the [CHTf<sub>2</sub>]<sup>-</sup> anion.

charge of the methanide carbon atom so that the total charge was +1 e. The Lennard-Jones parameters for the methanide group were those used in the literature for aromatic systems.<sup>55</sup> They were scaled to remove double counting of induction effects when introducing polarisation via Drude induced dipoles, following CL&Pol methodology<sup>40,53</sup> with the same scaling factors,  $\kappa_{[\text{C}_2\text{C}_1\text{Im}]^+-\text{Anion}^-} = 0.65$  and  $\kappa_{\text{C}_4\text{H}_{10}-\text{Anion}^-} = 0.77$ , as for [NTf<sub>2</sub>]<sup>-</sup>.<sup>56</sup>

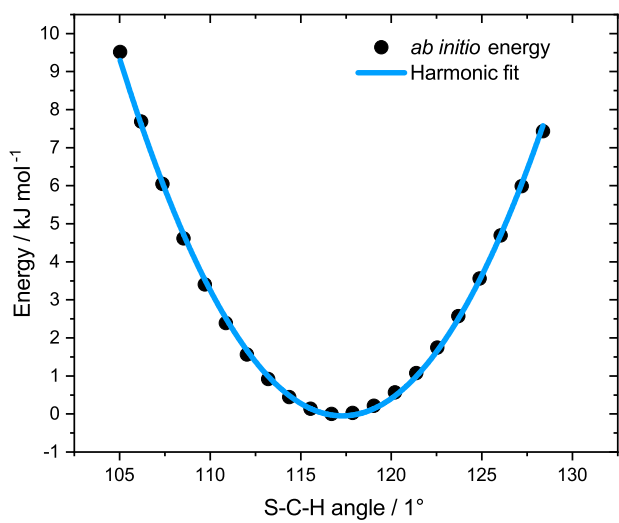
Bond stretching constants for C-F, F<sub>3</sub>C-S and S-O; angle bending constants for F-C-F, F-C-S, O-S-O and F<sub>3</sub>C-S-O; and dihedral OPLS parameters for O-S-C-F, C-S-C-F and O-S-C-S were taken from the [NTf<sub>2</sub>]<sup>-</sup> force field. C-H and C-S harmonic bond stretching constants involving the methanide group; harmonic angle bending constants for C-S-O, C-S-C, S-C-S and S-C-H; and OPLS dihedral constants for S-C-S-C and the improper S-S-C-H were obtained by fitting the full MP2/cc-pVTZ//B3LYP-GD3BJ/6-311+G(d,p) potential energy surface, Figure 8 (harmonic bond stretching), Figure 9 (harmonic angle bending) and Figure 10 (improper dihedral). Figure 11 shows the two-dimensional fit of the backbone dihedral. All the quantum calculations were performed using the Gaussian 09 software package.<sup>57</sup>



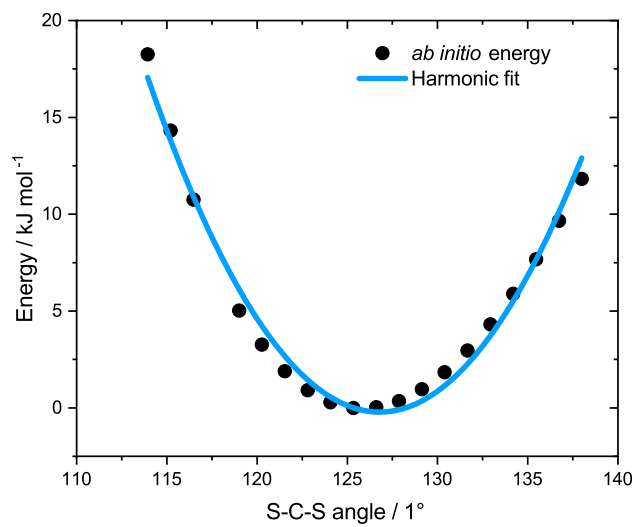
(a)



(b)



(c)



(d)

Figure 9: Fits for angle bending constants in the  $[\text{CHTf}_2]^-$  anion.

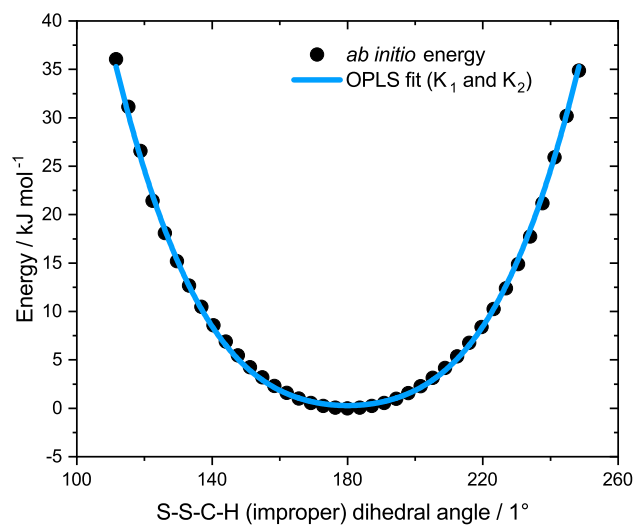


Figure 10: Fit of the improper dihedral S-S-C-H.

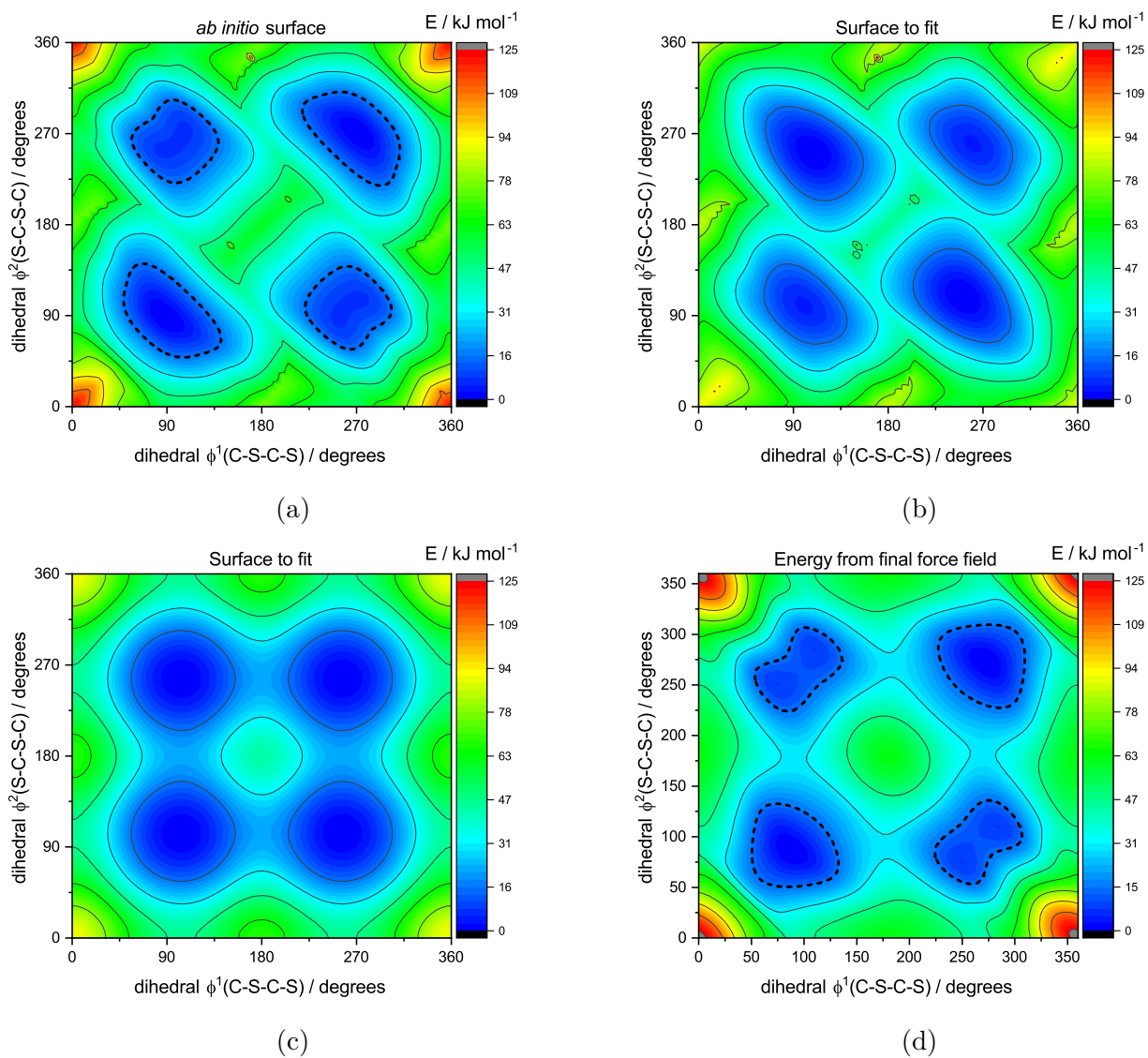


Figure 11: Two-dimensional fit of the backbone dihedral. a) *ab initio* target surface, b) difference surface to be fitted, c) final fit, d) Potential energy surface of the final force field.

### 5.3 Structure, Diffusion, and Heterogeneity

The structure of isotropic liquids is commonly characterised *via* radial distribution functions  $g^{\alpha\beta}(r)$ , Equation 7.<sup>58,59</sup>  $g^{\alpha\beta}(r)$  can be calculated by counting the number  $dn_{\beta}(r)$  of all particles  $j$  of type  $\beta$  in a shell of radius  $r$  and thickness  $dr$  around a central reference particle  $i$  (of type  $\alpha$ ). The ensemble average of  $n$  normalised by the number of particles in the spherical shell based on the ideal density  $\rho = N/V$  yields  $g^{\alpha\beta}(r)$ , Equation 8.<sup>58,60</sup> The particles  $i$  and  $j$  need not be atoms. For example, it is common practise to use the centre of mass or centre of charge vicariously for the position of a molecule.

$$g^{\alpha\beta}(r) = \frac{V}{N^2} \left\langle \sum_{i \neq j} \delta(\vec{r} - \vec{r}_{ij}) \right\rangle \quad (7)$$

$$g^{\alpha\beta}(r) \approx \frac{\langle dn_j(r) \rangle}{\rho 4\pi r^2 dr} \quad (8)$$

Atoms can scatter electromagnetic radiation of appropriate wavelength (X-rays) as well as neutrons or electrons. The scattered spherical waves of neighbouring atoms may interact constructively or destructively in certain locations, depending on the phase shift between them. Such methods can be used to probe or describe the liquid structure. The partial structure factor can in principle be calculated from the corresponding radial distribution function, Equation 9.<sup>59</sup> For an isotropic and homogeneous sample, this gives Equation 10.<sup>61,62</sup> Thus, for  $n$  distinguishable sites,  $n(n+1)/2$  partial structure factors define the (statistical) liquid structure.<sup>59</sup>

$$S^{\alpha\beta}(\vec{k}) = x_{\alpha}\delta_{\alpha\beta} + x_{\alpha}x_{\beta}\rho \int g^{\alpha\beta}(r)e^{-i\vec{k}\cdot\vec{r}} d\vec{r} \quad (9)$$

$$S^{\alpha\beta}(k) = x_{\alpha}\delta_{\alpha\beta} + x_{\alpha}x_{\beta} \int_{\mathbb{R}^+} \frac{\sin(kr)}{kr} g^{\alpha\beta}(r)\rho 4\pi r^2 dr \quad (10)$$

The structure factor  $S(k)$  is the sum of all partial structure factors, Equation 11.<sup>59</sup> Here,  $f(k)$  are the relevant scattering cross sections, which may also show a dependence on the wave vector.<sup>63</sup> The structure factor can be observed experimentally, for example in a small angle X-ray scattering (SAXS) experiment, which gives insight into the liquid structure and relevant length scales. For ionic liquids, it is sensible to also consider the charge-charge correlation structure factor  $S_{Charge}$ , *i.e.* atomic charges are used to weight the partial structure factors instead of the scattering cross sections, Equation 12.<sup>59,64</sup> Thus,  $S_{Charge}$  reveals details of electrostatic screening and charge ordering. In this work, instead of atomic charges, we use  $\pm 1$  charges placed on the

centres of charge of the cations and anions to calculate  $S_{Charge}$ .

$$S(k) = \sum_{\alpha,\beta} f_{\alpha}(k) f_{\beta}(k) S^{\alpha\beta}(k) \quad (11)$$

$$S_{Charge}(k) = \sum_{\alpha,\beta} q_{\alpha} q_{\beta} S^{\alpha\beta}(k) \quad (12)$$

The structure factors above were presented in real space for illustrative purposes. In practise, the structure factors are calculated directly in reciprocal space. Equation 13 and Equation 14 define the (dynamic) charge-charge correlation structure factor  $S_{Charge}(k, t)$ , Equation 15 and Equation 16 define the (dynamic) scattering structure factor  $S_{NN}(k, t)$ . See also Equations (1) to (4) in Reference [64].

$$S_{Charge}(\vec{k}, t) = S_{ZZ}(\vec{k}, t) = \frac{1}{V} \langle \hat{\rho}_Z(\vec{k}, t) \hat{\rho}_Z(-\vec{k}, 0) \rangle \quad (13)$$

$$\hat{\rho}_Z(\vec{k}, t) = \sum_{i=1}^N q_i e^{i\vec{k} \cdot \vec{r}_i(t)} \quad (14)$$

$$S_{X-ray}(k, t) = S_{NN}(\vec{k}, t) = \frac{1}{V} \langle \hat{\rho}_N(\vec{k}, t) \hat{\rho}_N(-\vec{k}, 0) \rangle \quad (15)$$

$$\hat{\rho}_N(\vec{k}, t) = \sum_{i=1}^N f_i(\vec{k}) e^{i\vec{k} \cdot \vec{r}_i(t)} \quad (16)$$

Here,  $\vec{k}$  is the momentum transfer variable,  $V$  is the volume, and  $\langle \dots \rangle$  is an ensemble average. Technically, the sum in Equation 14 runs over all atoms/particles  $i$  in the liquid with partial charges  $q_i$ , but in this work we compute the charge density on a coarser ion-by-ion level. Thus, we take the sum in Equation 14 to run over the centres of charge of each molecular ion, with corresponding ion charges  $q_i = \pm 1$ .

For computational efficiency, the reciprocal space charge density in Equation 14 is computed using beta-spline interpolation onto a grid followed by fast Fourier transform (FFT). This is analogous to the approach employed in the well-known particle-mesh Ewald method.<sup>65</sup> The details for this method of computing the scattering function have been previously described.<sup>64</sup>

Radial distribution functions can easily be extended to include dynamic behaviour. This leads to the van Hove function  $G(r, t)$ , Equation 17.<sup>59,66</sup> The van Hove function can be separated into a self part  $G_s(r, t)$  (18) and a distinct part  $G_d(r, t)$  (19).<sup>59</sup> The van Hove function can also be used to obtain a dynamic structure factor  $S(k, t)$ , fully analogous to the radial

distribution function.<sup>1</sup>

$$G(\vec{r}, t) = G_s(\vec{r}, t) + G_d(\vec{r}, t) \quad (17)$$

$$G_s(\vec{r}, t) = \frac{1}{N} \left\langle \sum_i \delta(\vec{r} + \vec{r}_i(0) - \vec{r}_i(t)) \right\rangle \quad (18)$$

$$G_d(\vec{r}, t) = \frac{1}{N} \left\langle \sum_{i \neq j} \delta(\vec{r} + \vec{r}_i(0) - \vec{r}_j(t)) \right\rangle \quad (19)$$

The van Hove function is calculated similar to the radial distribution function, only that the particle positions are compared at different times  $t$ . Thus, the distinct part at  $t = 0$  corresponds to the radial distribution function, *i.e.*  $G(r, 0) = \rho g(r)$ , see also Equation 7 compared to Equation 19.<sup>59</sup> In contrast, the self part at  $t = 0$  is trivial; it corresponds to a  $\delta$  function centred at the particle position. This initial  $\delta$  function broadens over time due to thermal motion, postulating Gaussian broadening gives Equation 20.<sup>59</sup> For freely moving particles obeying a Maxwell-Boltzmann distribution,  $\alpha(t)$  takes the form in Equation 21.<sup>59</sup> Similarly, in the case of normal Gaussian diffusion, Equation 20 is valid with Equation 22.<sup>59</sup> Here,  $d$  is the dimensionality of the system.

$$G_s(r, t) = \left( \frac{\alpha(t)}{\pi} \right)^{\frac{3}{2}} e^{-\alpha(t)r^2} \quad (20)$$

$$\alpha(t) = \frac{m}{2k_B T t^2} \quad (\text{ballistic}) \quad (21)$$

$$\alpha(t) = \frac{3}{4dD_{self}t} \quad (\text{hydrodynamic}) \quad (22)$$

If the behaviour is truly Gaussian, then the second and fourth moment of the distribution are given analytically by the blue part in Equation 23 and 24, respectively.<sup>59</sup> The mean squared displacement  $\langle(\Delta r)^2\rangle$  and the mean quartic displacement  $\langle(\Delta r)^4\rangle$  are readily accessible from an MD simulation. Thus, Equation 23 in combination with Equation 22 is the preferred way of calculating self-diffusion coefficients, which we also follow in this work. The components in  $x$ ,  $y$  and  $z$  direction can be determined independently, thus allowing for a simple error estimate from the difference between diffusion coefficients.<sup>67</sup> Figure 12 shows a log-log plot of the mean squared displacement of the anion in  $[C_4C_1im][NTf_2]$ . Two linear regions emerge, corresponding to the ballistic and the diffusive regimes, respectively. Caging and dynamical heterogeneity occur on the intermediate timescale between these two regimes.

---

<sup>1</sup>Technically the spatial Fourier transform of  $G(r, t)$  would be the intermediate scattering function  $F(k, t)$ , however the terminology is very fluid.

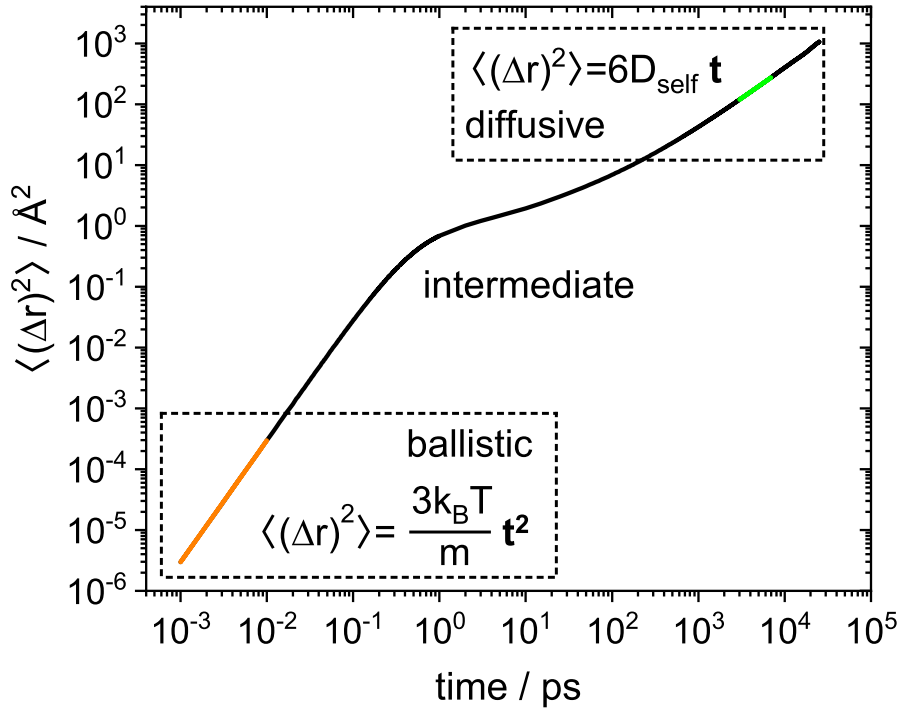


Figure 12: Mean squared displacement of the anions in a simulation of  $[\text{C}_4\text{C}_1\text{im}][\text{NTf}_2]$  (CL&Pol/TG-NH) at 333 K. The fitted region from 3-7 ns is highlighted in green and corresponds to 16% of the total simulation time.

$$\int_{\mathbb{R}^3} r^2 G_s(r, t) d\vec{r} = \langle(\Delta r)^2\rangle = \frac{3}{2\alpha(t)} \quad (23)$$

$$\int_{\mathbb{R}^3} r^4 G_s(r, t) d\vec{r} = \langle(\Delta r)^4\rangle = \frac{15}{4\alpha(t)^2} \quad (24)$$

It is possible for a system to show non-Gaussian behaviour, *i.e.* deviations from Equation 20. These deviations are commonly quantified with the non-Gaussian parameter  $\alpha_2(t)$ , Equation 25.<sup>68,69</sup> The non-Gaussian parameter takes nonzero values if  $G_s(r, t)$  deviates from a Gaussian profile, such behaviour is well documented for glass-forming liquids.<sup>68,70,71</sup>

$$\alpha_2(t) = \frac{3 \langle(\Delta r)^4\rangle}{5 \langle(\Delta r)^2\rangle^2} - 1 \quad (25)$$

For ionic liquids, non-Gaussian behaviour occurs usually on timescales of a few 100 ps, although the actual timescale depends on the conditions such as temperature and the system which is studied.<sup>72-75</sup> This behaviour is often interpreted as signature of dynamical heterogeneity, *i.e.* spatial regions with different timescales of relaxation.<sup>72,73,76-80</sup> Related to this is the ion cage interpretation, *i.e.* ions rattling in a cage of counter ions, with occasional jumps or hopping from one cage to a new one.<sup>30,70,72,77,78,81-84</sup> These two predominant explanations of non-Gaussian behaviour, dynamical heterogeneity and ion cage formation, are both important

concepts for ionic liquids. There is considerable overlap between the two explanations, and it is likely that they describe the same part of reality. For example, the region of a hopping ion is a region of faster relaxation, and *vice versa* for a caged ion. However, for ionic liquids, different timescales of relaxation can also occur within one molecular ion. The octopus effect refers to the phenomenon that alkyl side chains of a molecular ion often show faster local dynamics than the charged parts.<sup>75</sup> On long timescales, apolar (alkyl) and polar (charged) sites must of course diffuse together, thus the Gaussian behaviour is recovered.

The charge network formed by polar sites is another recurring theme in the discussion of non-Gaussian behaviour in ionic liquids. The slow relaxation of the (stiff) charge network eventually dominates the dynamics, in particular viscous flow.<sup>74,75,78,82,85-88</sup> Thus, knowledge of timescales of relaxation is of critical importance if one wishes to optimise the viscosity. For example, if the timescale of conformational changes is much slower than the lifetime of an ion cage, then the molecular ion effectively behaves as rigid. The timescales of dynamical heterogeneity and diffusion are given by the behaviour of  $\alpha_2(t)$  and  $\langle(\Delta r)^2\rangle$ , respectively. The dynamic charge-charge correlation structure factor  $S_{Charge}(k, t)$ , Equation 13 and Equation 14, can be used to obtain the timescale of charge network relaxation.

The anion diffusion coefficients in deliberately biased simulations were used in the main manuscript to distinguish between the effects of conformational flexibility (ease of interconversion between conformers) and the effects of preferred conformer (which conformer is the predominant one). For the sake of completeness, Figure 13 shows the corresponding cation diffusion coefficients.

## 5.4 Time Correlation Functions

The time correlation function formalism provides additional measure to describe conformational and orientational relaxation. Time correlation functions quantify the fluctuations of microscopic dynamic variables.<sup>60</sup> For example, consider the fluctuations  $\delta A(t)$  of a generic variable  $A(t)$  around its average value  $\langle A \rangle$ , Equation 26. The time correlation function  $C(t)$  is then defined as the ensemble (and time) average of the product between two fluctuations separated by the time interval  $t$ , Equation 27.<sup>89,90</sup> The normalised time correlation function can be used to define a lifetime  $\tau$ , Equation 28. Equation 28 is an analytical expression for the time constant if the decay is mono-exponential (*i.e.*  $C(t) = e^{-t/\tau}$ ), however also provides a robust estimate for

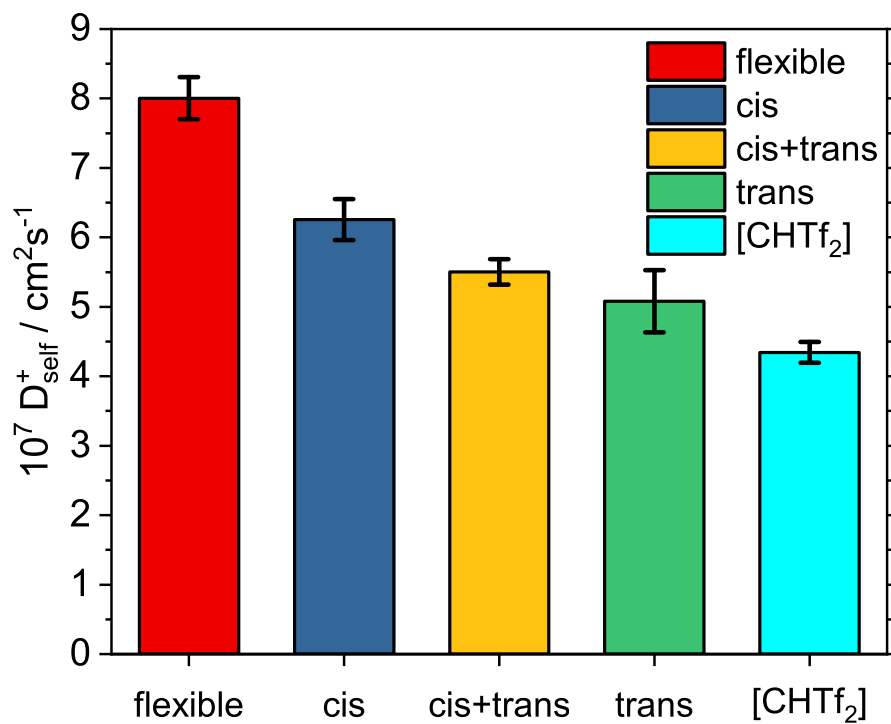


Figure 13: Cation self-diffusion coefficients obtained from MD simulations of native, flexible  $[\text{C}_4\text{C}_1\text{im}][\text{NTf}_2]$ , compared with targeted modifications where the anions in the simulation are restrained to cis/trans conformers. The cation diffusion coefficient of the ionic liquid  $[\text{C}_4\text{C}_1\text{im}][\text{CHTf}_2]$  is shown for comparison.

non-exponential or multi-exponential decay.

$$\delta A(t) = A(t) - \langle A \rangle = A(t) - \frac{1}{t'} \int_0^{t'} A(s) ds \quad (26)$$

$$C(t) = \langle A(0)A(t) \rangle = \frac{1}{t'} \int_0^{t'} \delta A(s) \delta A(s+t) ds \quad (27)$$

$$\tau = \int_{\mathbb{R}^+} \frac{C(t)}{C(0)} dt \quad (28)$$

In this work, conformational relaxation will be described with intermittent dihedral autocorrelation functions, Equation 29. One particular conformation of a molecule is usually defined by a set of geometric criteria, for example multiple dihedral angles which must take values within a certain range. The function  $h$  is one if these conditions are fulfilled, and zero otherwise. This binary approach was adopted from similar work on hydrogen bonding, where the hydrogen bond is defined by a set of distance and angle criteria.<sup>91,92</sup>

$$C_{dih}(t) = \frac{\langle \delta h(t) \delta h(0) \rangle}{\langle \delta h(0) \delta h(0) \rangle} = \frac{\langle (h(t) - \langle h \rangle)(h(0) - \langle h \rangle) \rangle}{\langle (h(0) - \langle h \rangle)^2 \rangle} \quad (29)$$

To measure orientational relaxation, it is common to define a vector in a molecule and trace the time evolution of this vector using a set of orientational correlation functions  $C_l(t)$ , Equation 30.<sup>59</sup> Here,  $\vec{u}$  is the unit vector representing the orientation of the molecule, this vector changes orientation by an angle  $\theta$  during the time  $t$ . The orientations are expanded in spherical harmonics, thus  $P_l$  are the Legendre polynomials of order  $l$ . This form of expansion conveniently decays to zero if the angles  $\theta$  are randomly distributed, and is already normalised, *i.e.*  $C_l(0) = 1$ . The first and second Legendre polynomials are of practical importance, see Equation 31 and 32.<sup>59,93</sup>

$$C_l(t) = \langle P_l(\vec{u}(t) \cdot \vec{u}(0)) \rangle \quad (30)$$

$$C_1(t) = \langle \cos(\theta(t)) \rangle \quad (31)$$

$$C_2(t) = \left\langle \frac{3 \cos^2(\theta(t)) - 1}{2} \right\rangle \quad (32)$$

## 5.5 Conformational Space

The key difference between  $[\text{CHTF}_2]^-$  and  $[\text{NTf}_2]^-$  lies in the accessible conformational space. The anion conformation is described by the two backbone dihedrals, and the conformer distribution in the bulk was hence obtained by binning these dihedral angles into a histogram, Figure 14. Here, for a structure to be classed as *trans*, both dihedral angles must either be in the range  $0^\circ$

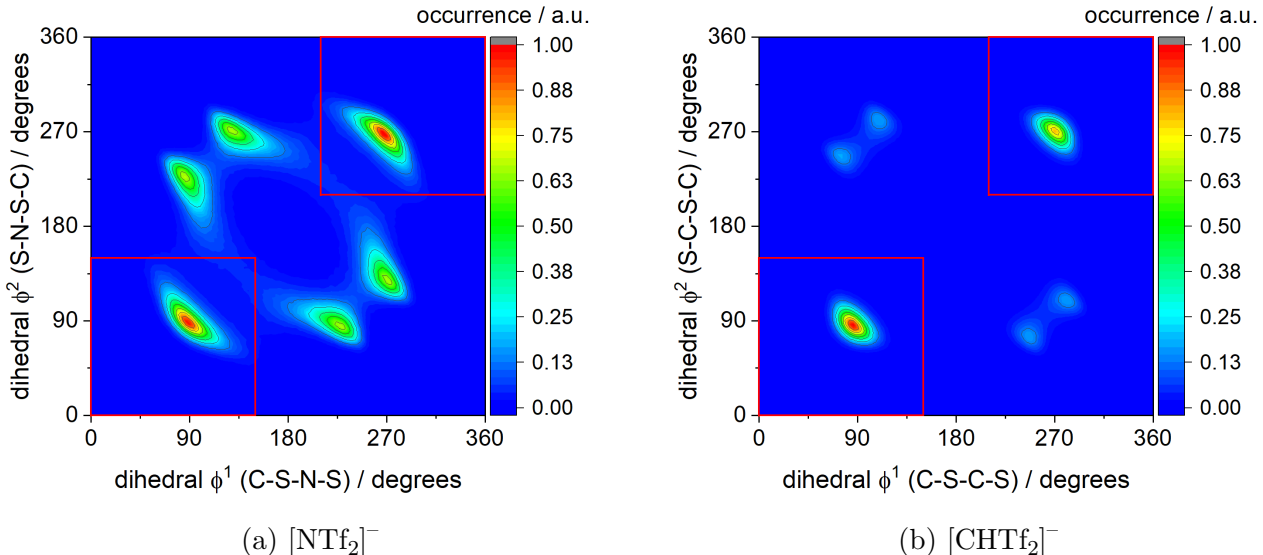


Figure 14: Histogram of anion geometries in simulation of (a)  $[C_4C_1im][NTf_2]$  and (b)  $[C_4C_1im][CHTf_2]$  at 298 K, normalised by the largest value.

to  $150^\circ$ , or in the range  $210^\circ$  to  $360^\circ$ . All other values were classed as *cis*. This choice of dihedral angle criteria corresponds to the red boxes in Figure 14, and was used to define the binary  $h$  in Equation 29. For  $[C_4C_1im][NTf_2]$ , the *cis* conformer was more common, with approximately 38% of the anions in the *trans* conformer both at 298 K and 333 K. For  $[C_4C_1im][CHTf_2]$ , the equilibrium was tipped towards the *trans* conformer. Statistically, 71% of the  $[CHTf_2]^-$  anions were *trans* at 298 K, which slightly decreased to 67% at 333 K.

## 5.6 Charge Arm ("Dipole Moment")

The properties of ionic liquids are defined by the strong intermolecular electrostatic interactions. Measures such as  $S_{Charge}(k)$  are useful to describe the charge network, but not the orientation dependence. The dipole moment (and higher order multipole moments) is more appropriate for this purpose. In practise, the dipole moment description is commonly used in theoretical studies on ionic liquids, despite its limitations.<sup>94–100</sup> While the dipole moment is well defined for neutral molecules, this is not the case for molecular ions. Only the first non-vanishing multipole moment is invariant to the choice of the origin of the coordinate system.<sup>101</sup> Hence, the concepts of charge arm and charge lever moment will be introduced in the following.<sup>94,102–104</sup> These quantities enable the discussion of rotational-translational coupling and provide well defined vectors for orientational relaxation.<sup>103</sup>

The dipole moment  $\vec{\mu}$  for a collection of point charges - such as the atomic sites of a

molecular ion in an MD simulation - is defined as the sum of the charge weighted positions, Equation 33.<sup>105</sup> Dividing this quantity by the total charge  $Q = \sum q_i$  of the molecular ion gives the centre of charge  $\vec{R}_{cq}$ , Equation 34. The similarity to the centre of mass  $\vec{R}_{cm}$ , Equation 35, is immediately evident. When constructing  $S_{Charge}(k)$  and  $E_{Coulomb}(r)$  from molecular point charges, it is reasonable to use  $\vec{R}_{cq}$  rather than  $\vec{R}_{cm}$ , thus eliminating the dipole term by definition.<sup>102,103</sup>

$$\vec{\mu} = \sum_i q_i \vec{x}_i \quad (33)$$

$$\vec{R}_{cq} = \frac{1}{Q} \sum_i q_i \vec{x}_i \quad (34)$$

$$\vec{R}_{cm} = \frac{1}{M} \sum_i m_i \vec{x}_i \quad (35)$$

For almost all ion types used in ionic liquids,  $\vec{R}_{cq}$  and  $\vec{R}_{cm}$  do not coincide, but are separated by a vector  $\vec{l}_q = \vec{R}_{cq} - \vec{R}_{cm}$ . The electrostatic interaction between the two ions acts on the centre of charge, however inertia  $I$  acts on the centre of mass. The charge arm  $L_C = |\vec{L}_C|$  of an ion is defined in analogy to a dipole moment with the centre of mass in the origin of the coordinate system, Equation 36.<sup>102</sup> Thus, the charge arm vectors tend to align, similar to the dipole moments in neutral molecules. The result is a torque  $\tau$  on the ions proportional to  $\vec{L}_C$ .<sup>2</sup> The torque results in an angular acceleration of  $\alpha = \tau/I$ . Hence, the angular acceleration is proportional to the charge lever moment  $Z$ , Equation 37, which in turn depends on the charge arm length  $L_C$  and the radius of gyration  $R_{gy}$ .<sup>103</sup>

$$\vec{L}_C = Q\vec{l}_q = Q(\vec{R}_{cq} - \vec{R}_{cm}) \quad (36)$$

$$Z = \frac{L_C}{MR_{gy}^2} \quad (37)$$

Knowledge about the magnitude of charge arm and charge lever moment and the timescale of their orientational relaxation is important since charge asymmetry provides additional pathways of structural reorganisation in ionic liquids. Rotational-translational coupling has been reported for ionic liquids as well as for related systems such as deep eutectic solvents or organic ionic plastic crystals.<sup>106-109</sup>

Bending of the S-N-S angle distorts the  $[\text{NTf}_2]^-$  *trans* structure from  $C_{2h}$  symmetry, for which the charge arm ('dipole moment' with the centre of mass as origin) would vanish due to

---

<sup>2</sup>Assuming spherical ions in a frictionless environment and an angle of 90° between force and  $\vec{L}_C$ .

the presence of an inversion centre. For this reason, the *trans* conformers have  $C_2$  symmetry and showed a very short charge arm around 0.1 Å, Table 16. In contrast, the *cis* structure is obtained by distorting the TS2 structure (which connects the two *cis* conformers). The TS2 has  $C_s$  symmetry, which allows for a non-vanishing charge arm. Hence, the charge arm for the *cis* conformers was ten times longer than for the *trans* conformer, around 1 Å, Table 16.

Table 16: Charge arms for different anions in the gas phase at the MP2/cc-pVTZ//RB3LYP-GD3BJ/6-311+G(d,p) level of theory. The [6 cPFSI]<sup>-</sup> anion is included for comparison as a type of anion which is locked in a *cis* conformation.

	$L_C$ / Debye		$L_C$ / eÅ	
	<i>cis</i>	<i>trans</i>	<i>cis</i>	<i>trans</i>
[CHTf <sub>2</sub> ] <sup>-</sup>	4.85	0.40	1.01	0.08
[NTf <sub>2</sub> ] <sup>-</sup>	4.71	0.35	0.98	0.07
[6 cPFSI] <sup>-</sup>	5.10	—	1.06	—

The strong correlation between conformation and charge arm was reflected in the charge arm distribution of the anions in the liquid. A bimodal distribution was obtained for the histogram of the anion charge arm lengths obtained from the simulations at 298 K, Figure 15a. The peaks at shorter charge arms correspond to the *trans* conformers, and those at longer charge arms correspond to the *cis* conformers. In agreement with Figure 14, shorter (longer) charge arms occurred more frequently for [CHTf<sub>2</sub>]<sup>-</sup> ([NTf<sub>2</sub>]<sup>-</sup>).

The probability  $p(L_C)$  of finding a charge arm of length  $L_C$  in a given bin of the histogram in Figure 15a can be used to obtain an estimate of the free energy  $F_{MD} = -RT \ln(p)$ , Figure 15b. The shallow free energy surface for the anion charge arm in [C<sub>4</sub>C<sub>1</sub>im][NTf<sub>2</sub>]<sup>-</sup> - a direct result of the shallow free energy surface of the conformational space - means that the [NTf<sub>2</sub>]<sup>-</sup> anion can react dynamically to changes in the electrostatic environment. This is desirable to accelerate structural relaxation and decrease viscosity.

## 5.7 Charge Network relaxation times

A tri exponential fit of  $S_{Charge}(k, t)$  was used to obtain estimates of the charge network lifetimes for quantitative comparison, Equation 38, with the constraint  $A_1 + A_2 + A_3 = 1$ . The fit was performed at the position of the charge network peak,  $k_{max} \approx 0.8 \text{ Å}^{-1}$ . The charge network

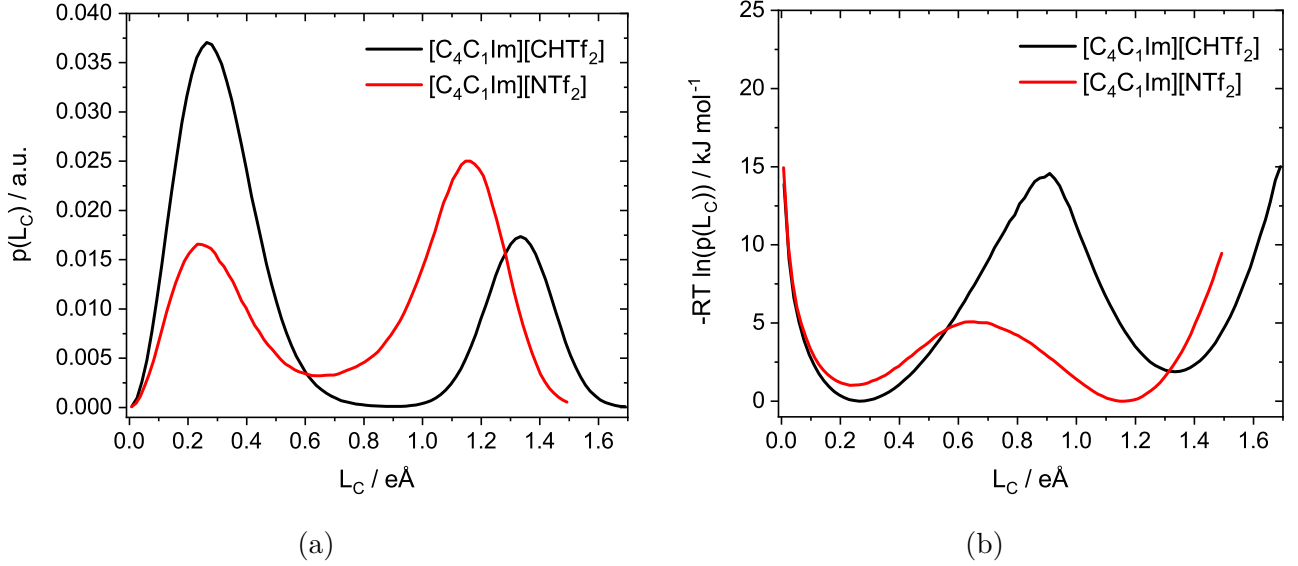


Figure 15: (a) Anion charge arm histogram and (b) corresponding potential of mean force for CL&Pol/TG-NH simulations at 298 K.

lifetime  $\tau_{ZZ}$  was then obtained *via* Equation 39.

$$S_{Charge}(k_{max}, t) = S_{Charge}(k_{max}, 0) (A_1 e^{-t/\tau_1} + A_2 e^{-t/\tau_2} + A_3 e^{-t/\tau_3}) \quad (38)$$

$$\tau_{ZZ} = A_1 \tau_1 + A_2 \tau_2 + A_3 \tau_3 \quad (39)$$

The lifetimes thus obtained are given in Table 17. It is evident that  $\tau_{ZZ}$  was significantly higher for  $[C_4C_1im][CHTf_2]$  compared to  $[C_4C_1im][NTf_2]$  by a factor of 1.59 at both temperatures. However, the effect of temperature on the charge network lifetimes was even more pronounced. The lifetimes were higher by a factor of  $\tau_{ZZ}(298\text{ K})/\tau_{ZZ}(333\text{ K}) = 3.58$  for both ionic liquids. Yet again, this observation shows that conformational flexibility gives relaxation mechanisms a ‘head start’ in the  $[C_4C_1im][NTf_2]$  ionic liquid, which is particularly important at low temperatures.

Table 17: Charge network relaxation times obtained following Equation 39.

	$T$	$\tau_{ZZ} / \text{ps}$	$\Delta\tau_{ZZ} / \text{ps}$	$\tau_{ZZ}^{298\text{ K}} / \tau_{ZZ}^{333\text{ K}}$
$[C_4C_1im][NTf_2]$	298 K	1020	8	3.579
	333 K	285	5	
$[C_4C_1im][CHTf_2]$	298 K	1621	8	3.586
	333 K	452	8	

## References

- (1) C. Reichardt and T. Welton, *Solvents and Solvent Effects in Organic Chemistry*, Wiley-VCH Verlag GmbH & Co. KGaA, Weinheim, Germany, 4th edn., 2010.
- (2) M. Hesse, H. Meier and B. Zeeh, *Spektroskopische Methoden in der organischen Chemie*, Georg Thieme Verlag, Stuttgart, 8th edn., 2012.
- (3) F. Philippi, D. Rauber, B. Kuttich, T. Kraus, C. W. M. Kay, R. Hempelmann, P. A. Hunt and T. Welton, *Physical Chemistry Chemical Physics*, 2020, **22**, 23038–23056.
- (4) B. Helferich and H. Grünert, *Berichte der deutschen chemischen Gesellschaft (A and B Series)*, 1940, **73**, 1131–1133.
- (5) J. M. Pringle, J. Golding, K. Baranyai, C. M. Forsyth, G. B. Deacon, J. L. Scott and D. R. MacFarlane, *New J. Chem.*, 2003, **27**, 1504–1510.
- (6) Y. Jeong, J. Ban, M. Lim and H. Rhee, *Synthesis*, 2018, **50**, 1867–1874.
- (7) M. T. Martin, F. Roschangar and J. F. Eaddy, *Tetrahedron Letters*, 2003, **44**, 5461–5463.
- (8) H. Zhang, U. Oteo, H. Zhu, X. Judez, M. Martinez-Ibañez, I. Aldalur, E. Sanchez-Diez, C. Li, J. Carrasco, M. Forsyth and M. Armand, *Angewandte Chemie International Edition*, 2019, **58**, 7829–7834.
- (9) J. L. Ferguson, J. D. Holbrey, S. Ng, N. V. Plechkova, K. R. Seddon, A. a. Tomaszowska and D. F. Wassell, *Pure and Applied Chemistry*, 2011, **84**, 723–744.
- (10) Agilent, *CrysAlis PRO*, Yarnton, Oxfordshire, England, 2014.
- (11) O. V. Dolomanov, L. J. Bourhis, R. J. Gildea, J. A. K. Howard and H. Puschmann, *Journal of Applied Crystallography*, 2009, **42**, 339–341.
- (12) C. F. Macrae, I. Sovago, S. J. Cottrell, P. T. A. Galek, P. McCabe, E. Pidcock, M. Platings, G. P. Shields, J. S. Stevens, M. Towler and P. A. Wood, *Journal of Applied Crystallography*, 2020, **53**, 226–235.
- (13) F. Philippi, D. Pugh, D. Rauber, T. Welton and P. A. Hunt, *Chemical Science*, 2020, **11**, 6405–6422.
- (14) G. A. Jeffrey, *An Introduction to Hydrogen Bonding*, Oxford University Press, New York, 1997.

- (15) T. Steiner, *Angewandte Chemie International Edition*, 2002, **41**, 48–76.
- (16) E. Gomez, N. Calvar, A. Dominguez and E. A. Macedo, *Industrial & Engineering Chemistry Research*, 2013, **52**, 2103–2110.
- (17) K. R. Harris and M. Kanakubo, *Physical Chemistry Chemical Physics*, 2015, **17**, 23977–23993.
- (18) Z. J. Chen, T. Xue and J.-M. Lee, *RSC Advances*, 2012, **2**, 10564.
- (19) K. R. Harris, M. Kanakubo and L. A. Woolf, *Journal of Chemical and Engineering Data*, 2007, **52**, 1080–1085.
- (20) M. Kanakubo, K. R. Harris, N. Tsuchihashi, K. Ibuki and M. Ueno, *Journal of Chemical & Engineering Data*, 2015, **60**, 1495–1503.
- (21) O. Palumbo, F. Trequattrini, F. M. Vitucci and A. Paolone, *The Journal of Physical Chemistry B*, 2015, **119**, 12905–12911.
- (22) O. Palumbo, F. Trequattrini, G. Appetecchi, L. Conte and A. Paolone, *Journal of Molecular Liquids*, 2017, **243**, 9–13.
- (23) T. Yamaguchi, S. Miyake and S. Koda, *The Journal of Physical Chemistry B*, 2010, **114**, 8126–8133.
- (24) W. Makino, R. Kishikawa, M. Mizoshiri, S. Takeda and M. Yao, *The Journal of Chemical Physics*, 2008, **129**, 104510.
- (25) A. S. Nowick, B. S. Berry and J. L. Katz, *Anelastic Relaxation in Crystalline Solids*, Academic Press, New York and London, 1972.
- (26) G. S. Fulcher, *Journal of the American Ceramic Society*, 1925, **8**, 339–355.
- (27) G. Tammann and W. Hesse, *Zeitschrift für anorganische und allgemeine Chemie*, 1926, **156**, 245–257.
- (28) D. H. Vogel, *Physikalische Zeitschrift*, 1921, **22**, 645.
- (29) O. Okoturo and T. VanderNoot, *Journal of Electroanalytical Chemistry*, 2004, **568**, 167–181.
- (30) M. Sha, X. Ma, N. Li, F. Luo, G. Zhu and M. D. Fayer, *The Journal of Chemical Physics*, 2019, **151**, 154502.

- (31) S. Cheng, Z. Wojnarowska, M. Musiał and M. Paluch, *The Journal of Chemical Physics*, 2021, **154**, 044502.
- (32) Y. Marcus, *Fluid Phase Equilibria*, 2014, **363**, 66–69.
- (33) A. F. Bouarab, J.-P. Harvey and C. Robelin, *Physical Chemistry Chemical Physics*, 2021, **23**, 733–752.
- (34) M. H. Ghatee, M. Zare, A. R. Zolghadr and F. Moosavi, *Fluid Phase Equilibria*, 2010, **291**, 188–194.
- (35) G. Cannelli, R. Cantelli, F. Cordero and F. Trequattrini, *Physical Review B*, 1997, **55**, 14865–14871.
- (36) F. Trequattrini, A. Paolone, O. Palumbo, F. Vitucci, M. Navarra and S. Panero, *Archives of Metallurgy and Materials*, 2015, **60**, 385–390.
- (37) H. Sun, *The Journal of Physical Chemistry B*, 1998, **102**, 7338–7364.
- (38) J.-P. Ryckaert, G. Ciccotti and H. J. Berendsen, *Journal of Computational Physics*, 1977, **23**, 327–341.
- (39) A. Dequidt, J. Devémy and A. A. H. Pádua, *Journal of Chemical Information and Modeling*, 2016, **56**, 260–268.
- (40) K. Goloviznina, J. N. Canongia Lopes, M. Costa Gomes and A. A. H. Pádua, *Journal of Chemical Theory and Computation*, 2019, **15**, 5858–5871.
- (41) E. Heid, A. Szabadi and C. Schröder, *Physical Chemistry Chemical Physics*, 2018, **20**, 10992–10996.
- (42) G. Lamoureux and B. Roux, *The Journal of Chemical Physics*, 2003, **119**, 3025–3039.
- (43) B. Thole, *Chemical Physics*, 1981, **59**, 341–350.
- (44) G. J. Martyna, D. J. Tobias and M. L. Klein, *The Journal of Chemical Physics*, 1994, **101**, 4177–4189.
- (45) C. Y. Son, J. G. McDaniel, Q. Cui and A. Yethiraj, *The Journal of Physical Chemistry Letters*, 2019, **10**, 7523–7530.
- (46) K. Goloviznina, Z. Gong, M. F. Costa Gomes and A. A. H. Pádua, *Journal of Chemical Theory and Computation*, 2021, **17**, 1606–1617.
- (47) The Plumed Consortium, *Nature Methods*, 2019, **16**, 670–673.

- (48) G. Bussi and G. A. Tribello, in *Methods in Molecular Biology*, 2019, vol. 2022, pp. 529–578.
- (49) G. A. Tribello, M. Bonomi, D. Branduardi, C. Camilloni and G. Bussi, *Computer Physics Communications*, 2014, **185**, 604–613.
- (50) L. Martínez, R. Andrade, E. G. Birgin and J. M. Martínez, *Journal of Computational Chemistry*, 2009, **30**, 2157–2164.
- (51) J. N. Canongia Lopes and A. A. H. Pádua, *The Journal of Physical Chemistry B*, 2004, **108**, 16893–16898.
- (52) A. S. L. Gouveia, C. E. S. Bernardes, L. C. Tomé, E. I. Lozinskaya, Y. S. Vygodskii, A. S. Shaplov, J. N. C. Lopes and I. M. Marrucho, *Physical Chemistry Chemical Physics*, 2017, **19**, 29617–29624.
- (53) A. A. H. Pádua, *The Journal of Chemical Physics*, 2017, **146**, 204501.
- (54) C. M. Breneman and K. B. Wiberg, *Journal of Computational Chemistry*, 1990, **11**, 361–373.
- (55) J. N. Canongia Lopes and A. A. H. Pádua, *The Journal of Physical Chemistry B*, 2006, **110**, 19586–19592.
- (56) F. Philippi, K. Goloviznina, Z. Gong, S. Gehrke, B. Kirchner, A. A. H. Pádua and P. A. Hunt, *Physical Chemistry Chemical Physics*, 2022, **24**, 3144–3162.
- (57) M. J. Frisch and G. Trucks, *Gaussian 09*, Wallingford CT, 2016.
- (58) M. P. Allen and D. J. Tildesley, *Computer Simulation of Liquids*, Oxford University Press, 2nd edn., 2017, vol. 1.
- (59) J.-P. Hansen and I. R. McDonald, *Theory of Simple Liquids*, Elsevier, 4th edn., 2013.
- (60) F. Jensen, *Introduction to Computational Chemistry*, John Wiley & Sons, Inc., West Sussex, 2nd edn., 2007.
- (61) J. L. Yarnell, M. J. Katz, R. G. Wenzel and S. H. Koenig, *Physical Review A*, 1973, **7**, 2130–2144.
- (62) D. Chandler, *Introduction to modern statistical mechanics*, Oxford University Press, New York, 1987.

- (63) M. Brehm, M. Thomas, S. Gehrke and B. Kirchner, *The Journal of Chemical Physics*, 2020, **152**, 164105.
- (64) J. G. McDaniel and A. Yethiraj, *The Journal of Physical Chemistry B*, 2019, **123**, 3499–3512.
- (65) U. Essmann, L. Perera, M. L. Berkowitz, T. Darden, H. Lee and L. G. Pedersen, *The Journal of Chemical Physics*, 1995, **103**, 8577–8593.
- (66) L. Van Hove, *Physical Review*, 1954, **95**, 249–262.
- (67) E. J. Maginn, R. A. Messerly, D. J. Carlson, D. R. Roe and J. R. Elliott, *Living Journal of Computational Molecular Science*, 2019, **1**, 1–20.
- (68) B. Vorselaars, A. V. Lyulin, K. Karatasos and M. A. Michels, *Physical Review E - Statistical, Nonlinear, and Soft Matter Physics*, 2007, **75**, 011504.
- (69) A. Rahman, *Physical Review*, 1964, **136**, A405–A411.
- (70) B. P. Bhowmik, I. Tah and S. Karmakar, *Physical Review E*, 2018, **98**, 022122.
- (71) R. Richert, *Journal of Physics: Condensed Matter*, 2002, **14**, 201.
- (72) M. G. Del Pópolo and G. A. Voth, *The Journal of Physical Chemistry B*, 2004, **108**, 1744–1752.
- (73) T. Köddermann, R. Ludwig and D. Paschek, *ChemPhysChem*, 2008, **9**, 1851–1858.
- (74) W. D. Amith, J. C. Araque and C. J. Margulis, *The Journal of Physical Chemistry Letters*, 2020, **11**, 2062–2066.
- (75) R. P. Daly, J. C. Araque and C. J. Margulis, *The Journal of Chemical Physics*, 2017, **147**, 061102.
- (76) E. J. Maginn, *Journal of Physics: Condensed Matter*, 2009, **21**, 373101.
- (77) J. Habasaki and K. L. Ngai, *The Journal of Chemical Physics*, 2008, **129**, 194501.
- (78) J. C. Araque, S. K. Yadav, M. Shadeck, M. Maroncelli and C. J. Margulis, *The Journal of Physical Chemistry B*, 2015, **119**, 7015–7029.
- (79) M. Torkzadeh and M. Moosavi, *Journal of Molecular Liquids*, 2021, **330**, 115632.
- (80) Y. Wang, W. Jiang, T. Yan and G. A. Voth, *Accounts of Chemical Research*, 2007, **40**, 1193–1199.

- (81) J. C. Araque, R. P. Daly and C. J. Margulis, *The Journal of Chemical Physics*, 2016, **144**, 204504.
- (82) J. C. Araque, J. J. Hettige and C. J. Margulis, *The Journal of Physical Chemistry B*, 2015, **119**, 12727–12740.
- (83) M. Casalegno, G. Raos, G. B. Appetecchi, S. Passerini, F. Castiglione and A. Mele, *The Journal of Physical Chemistry Letters*, 2017, **8**, 5196–5202.
- (84) G. Feng, M. Chen, S. Bi, Z. A. Goodwin, E. B. Postnikov, N. Brilliantov, M. Urbakh and A. A. Kornyshev, *Physical Review X*, 2019, **9**, 021024.
- (85) T. Yamaguchi, *The Journal of Chemical Physics*, 2016, **145**, 194505.
- (86) T. Yamaguchi, *The Journal of Chemical Physics*, 2016, **144**, 124514.
- (87) T. Yamaguchi, *Physical Chemistry Chemical Physics*, 2018, **20**, 17809–17817.
- (88) J. C. Araque and C. J. Margulis, *The Journal of Chemical Physics*, 2018, **149**, 144503.
- (89) R. Zwanzig, *Nonequilibrium Statistical Mechanics*, Oxford University Press, New York, 2001.
- (90) B. Bagchi, *Molecular Relaxation in Liquids*, Oxford University Press, New York, 2012.
- (91) A. Luzar, *The Journal of Chemical Physics*, 2000, **113**, 10663–10675.
- (92) R. J. Gowers and P. Carbone, *The Journal of Chemical Physics*, 2015, **142**, 224907.
- (93) T. Pal and R. Biswas, *Theoretical Chemistry Accounts*, 2013, **132**, 1348.
- (94) M. N. Kobrak and H. Li, *Physical Chemistry Chemical Physics*, 2010, **12**, 1922.
- (95) C. A. Rumble, C. Uitvlugt, B. Conway and M. Maroncelli, *The Journal of Physical Chemistry B*, 2017, **121**, 5094–5109.
- (96) R. E. Ramírez, L. C. Torres-González, A. Hernández, A. García and E. M. Sánchez, *The Journal of Physical Chemistry B*, 2010, **114**, 4271–4275.
- (97) K. Wendler, F. Dommert, Y. Y. Zhao, R. Berger, C. Holm and L. Delle Site, *Faraday Discuss.*, 2012, **154**, 111–132.
- (98) E. I. Izgorodina, Z. L. Seeger, D. L. A. Scarborough and S. Y. S. Tan, *Chemical Reviews*, 2017, **117**, 6696–6754.
- (99) S. Koßmann, J. Thar, B. Kirchner, P. A. Hunt and T. Welton, *The Journal of Chemical Physics*, 2006, **124**, 174506.

- (100) B. D. Rabideau, M. Soltani, R. A. Parker, B. Siu, E. A. Salter, A. Wierzbicki, K. N. West and J. H. Davis, *Physical Chemistry Chemical Physics*, 2020, **22**, 12301–12311.
- (101) L. Piela, in *Ideas of Quantum Chemistry*, Elsevier, 2014, e169–e181.
- (102) M. N. Kobrak and N. Sandalow, *ECS Proceedings Volumes*, 2004, **2004-24**, 417–425.
- (103) H. Li, M. Ibrahim, I. Agberemi and M. N. Kobrak, *The Journal of Chemical Physics*, 2008, **129**, 124507.
- (104) F. Philippi and T. Welton, *Physical Chemistry Chemical Physics*, 2021, **23**, 6993–7021.
- (105) D. J. Griffiths, *Introduction to Electrodynamics*, Cambridge University Press, Cambridge, 2017.
- (106) D. Reuter, P. Münzner, C. Gainaru, P. Lunkenheimer, A. Loidl and R. Böhmer, *The Journal of Chemical Physics*, 2021, **154**, 154501.
- (107) P. Sippel, S. Krohns, D. Reuter, P. Lunkenheimer and A. Loidl, *Physical Review E*, 2018, **98**, 1–9.
- (108) K. Geirhos, P. Lunkenheimer, M. Michl, D. Reuter and A. Loidl, *The Journal of Chemical Physics*, 2015, **143**, 081101.
- (109) D. R. MacFarlane and M. Forsyth, *Advanced Materials*, 2001, **13**, 957–966.